ORCID Details:

https://orcid.org/0009-0001-2810-5336

DECLARATION

This manuscript has been submitted for publication in Journal of Climate Dynamics. Please note that, it is yet to undergo peer review and yet to be formally accepted for publication. Subsequent versions of this manuscript may have slightly different content. If accepted, the final version of this manuscript will be available via the 'Peer-reviewed Publication DOI' link on the right-hand side of this webpage. Please feel free to contact any of the authors; we welcome feedback.

Title of the Article:

MJO Phase-Response Diagnostic Skill Reflects Convective Regime Contingency Beyond Coupling Strength Across Tropical Sites

Author:

Mr Pochender Shenigarapu
Doctoral Research Scholar
Jawaharlal Nehru Technological University Anantapur
Anantapuramu – 515002
INDIA
pochender.ce.scholar@gprec.ac.in
Phone: +91-9949999277

Co Author:

Dr Prof. Sanjeeva Rayudu Ekkaluri
Asst. Professor
G Pulla Reddy Engineering College
Kurnool – 518007
INDIA
sanjeeva.ce@gprec.ac.in

Corresponding Author:

Mr Pochender Shenigarapu
pochender.ce.scholar@gprec.ac.in

MJO Phase-Response Diagnostic Skill Reflects Convective Regime Contingency Beyond Coupling Strength Across Tropical Sites

Abstract

MJO phase composites are the standard tool for building tropical rainfall diagnostic frameworks. The coupling strength between the MJO phase and local rainfall is routinely used to justify their application. Whether coupling strength alone guarantees diagnostic skill — or whether the nature of the underlying convective regime is the additional governing condition — has not been examined. We introduce CPA_{dry}, the Conditional Probability Anomaly for strongly suppressive MJO phases, and evaluate it across seven tropical sites spanning the Indo-Pacific and tropical Africa. Where the MJO exerts direct convective envelope control — Darwin ($\eta^2 = 7.5\%$) and Dili ($\eta^2 = 6.7\%$) — CPA_{dry} achieves robust precursor skill at 5–15 day lead times (AUC 0.69–0.76). Where remote teleconnections govern, or where MJO-rainfall coupling is structurally absent, skill is negligible regardless of coupling magnitude. The sharpest demonstration is Colombo — the strongest-coupled site ($\eta^2 = 11.2\%$) — which yields AUC indistinguishable from random (0.50). Coupling strength is necessary but insufficient. Convective regime contingency is the additional governing condition. These results formalise the active-versus-passive modulation principle: CPA_{dry} detects failures of direct local MJO inhibition but not the absence of remotely modulated convective enhancement. This asymmetry holds within individual sites — suppression failure AUC 0.69–0.76, enhancement failure AUC 0.52–0.55 — and is structural: a designed regime-conditioning falsification test failed to recover wet-phase skill (the best conditioned AUC was 0.569, with the remaining AUCs 0.06 below the rolling baseline). A coupling–contingency threshold near $\eta^2 \approx 5$–6% demarcates the transition from direct-envelope-passage to remote-teleconnection regimes. Below it, skill collapses to chance level regardless of coupling magnitude. Independent Bureau of Meteorology gauge validation at Darwin corroborates and modestly strengthens all reanalysis-derived estimates. Projected changes in MJO amplitude, propagation speed, and Maritime Continent barrier penetration under warming are likely to shift this threshold geographically — making the $\eta^2 \approx 5$–6% boundary condition a practical benchmark for monitoring the climate-driven evolution of MJO diagnostic utility.

Key words

Madden-Julian Oscillation, Phase-Response Diagnostics, Active-Passive Modulation, Coupling-Contingency, Conditional Probability Anomaly, Maritime Continent, Subseasonal Forecasting.

1. Introduction

Phase-conditioned rainfall diagnostics have become a cornerstone of subseasonal forecasting across the tropics and subtropics. Operational centres issue MJO phase-based precipitation outlooks routinely (Vitart, 2017; Lim et al., 2018; Tsai et al., 2025), and diagnostic frameworks use phase composites to identify periods of anomalous rainfall and elevated heavy-precipitation risk (Wheeler et al., 2009; Jones et al., 2004; Cowan et al., 2023). The foundation of this enterprise is the Madden-Julian Oscillation (MJO; Madden and Julian 1971, 1972) — the dominant mode of tropical intraseasonal variability, organising convective activity into an eastward-propagating envelope (Lau and Chan, 1986, *Mon Rev 114:1354-1367*) with a 30–90 day period. Its eight-phase classification, established by the Wheeler-Hendon Real-time Multivariate MJO index (Wheeler & Hendon, 2004), provides the phase architecture on which these diagnostics are built. The implicit governing assumption is that statistically significant MJO-rainfall coupling at a site is sufficient to justify the construction and operational deployment of phase-response diagnostic frameworks. This paper demonstrates that the assumption is incomplete.

The assumption rests on an important but unexamined distinction in how the MJO influences local rainfall. At sites where the MJO convective envelope passes directly overhead — the Maritime Continent, northern Australia, and adjacent Indo-Pacific regions — phase-rainfall coupling reflects direct convective modulation: suppressive phases deliver descending motion, reduced moisture convergence, and inhibited deep convection locally (Hendon and Liebmann, 1990; Wheeler and McBride, 2005; Wheeler et al., 2009; DeMott et al., 2015; Tsai et al., 2025). At many other tropical sites, however, the MJO's influence operates through remote pathways — modulation of Indian Ocean moisture flux (Annamalai and Slingo, 2001; Krishnamurthy & Shukla, 2007), alteration of the Walker circulation (Rui and Wang, 1990; Zhang, 2005), or suppression of oceanic evaporation over thousands of kilometres — mechanisms that are statistically detectable yet physically distinct from direct envelope passage (Woolnough et al., 2000)(*The relationship between convection and sea surface temperature on intraseasonal timescales. (J Atmos Sci 57:945-968*) The statistical coupling at remote-influence sites can be strong, even dominant by conventional measures. Yet the physical process governing that coupling is qualitatively different — and, as this paper demonstrates, that difference determines whether phase-response diagnostics retain or lose predictive skill.

This distinction has not been incorporated into MJO diagnostic frameworks. Phase-conditioned rainfall diagnostics are constructed and evaluated identically regardless of the physical mechanism governing local coupling — whether that coupling reflects direct convective envelope passage or a remote teleconnection pathway (Vitart and Robertson, 2018; Domeisen et al., 2020; Lim et al., 2018). Coupling strength, typically quantified as η^2 or composite rainfall anomaly magnitude, is treated as the sole criterion for diagnostic applicability (Gottschalck et al., 2010) (*A framework for assessing operational Madden-Julian Oscillation forecasts: a CLIVAR MJO Working Group project. Bull Am Meteorol Soc 91:1247-1258*). No framework in the current literature conditions diagnostic deployment on the type of MJO influence — only on its statistical strength (Wheeler et al., 2009). The reliability of published skill figures for MJO diagnostic frameworks has itself been called into question: Suematsu et al. (2024) demonstrated that a widely-cited machine learning MJO prediction study reported COR-based skill inflated by a factor of two to three due to an incorrect accumulative formulation, reducing apparent all-season skill from 26–27 days to 11–12 days. Methodological rigour in metric design is therefore a precondition for meaningful diagnostic comparison. This is not a refinement that the field has overlooked. It is a precondition for diagnostic skill that the field has yet to identify. The consequence is systematic: frameworks built on remote-teleconnection coupling may exhibit strong statistical association yet produce no usable predictive skill — a failure mode that conventional coupling metrics cannot detect and that the present study formalises for the first time across a seven-site tropical network.

We introduce CPA_{dry} — the Conditional Probability Anomaly for strongly suppressive MJO phases — to directly address this gap. CPA_{dry} measures the rate at which strongly suppressive MJO phases fail to inhibit local heavy convection, computed as a rolling conditional probability anomaly over a 60-day window centred on each target day. The metric is designed around a specific physical premise: where the MJO exerts direct local inhibitory control through descending-branch dynamics, suppression failure is a detectable and physically interpretable event — an override of the MJO's mechanistically grounded suppressive signal by competing local or synoptic-scale processes (DeMott et al., 2015; Kiladis et al., 2014; Roundy, 2012). Where the MJO's influence is remote and permissive rather than local and inhibitory, suppression failure is not a coherent physical category — there is no active inhibitory mechanism to override. CPA_{dry} therefore does not simply measure phase-rainfall association. It measures whether a physically grounded inhibitory process can be detected as failing — a fundamentally different diagnostic question from whether phase and rainfall are statistically correlated. The design explicitly targets suppressive rather than enhancing phases because inhibitory MJO

dynamics — reduced moisture convergence, enhanced 500 hPa subsidence, boundary layer drying — operate through a direct, locally acting mechanism whose failure carries diagnostic information (Hendon and Liebmann, 1990; Wheeler and McBride, 2005; DeMott et al., 2015). Enhancing phases do not carry the same mechanistic specificity at remote-influence sites, a distinction that the results confirm empirically.

We test CPA_{dry} across seven sites selected to span the full spectrum of MJO influence mechanisms — from direct convective envelope passage at Darwin (Australia) and Dili (Timor-Leste) through attenuated Maritime Continent influence at Makassar (Indonesia) and Port Moresby (Papua New Guinea), to remote teleconnection regimes at Colombo (Sri Lanka) and Mombasa (Kenya), and structurally absent coupling at Niamey (Niger). This design is deliberate. A seven-site network spanning three distinct MJO influence regimes provides the geographic and physical diversity necessary to test whether coupling type — not merely coupling strength — governs diagnostic skill. The central finding is a coupling-contingency threshold near $\eta^2 \approx 5–6\%$, demarcating the transition from direct-envelope-passage to remote-teleconnection regimes. Below this threshold, CPA_{dry} skill collapses to chance level regardless of coupling magnitude. The sharpest demonstration is Colombo — the strongest-coupled site in the network ($\eta^2 = 11.2\%$) — which yields AUC indistinguishable from random (0.50). No existing diagnostic framework predicts this result. η^2 alone cannot detect it. The finding exposes a structural gap in the field's current approach to diagnostic applicability assessment (Vitart and Robertson, 2018; Domeisen et al., 2020; Wheeler et al., 2009). A second dimension of the contribution operates within individual sites. At Darwin and Dili, suppression failure is robustly detectable (AUC 0.69–0.76). Enhancement failure — the failure of wet phases to deliver expected heavy rainfall — is not (AUC 0.52–0.55) and remains unrecoverable through regime conditioning. This within-site asymmetry mirrors the across-site pattern and is unified by the same principle: CPA_{dry} detects failures of active local inhibitory processes but not the withdrawal of remote permissive conditions. Together, these findings formalise the active-versus-passive modulation principle as a diagnostic boundary condition for MJO phase-response frameworks — a condition the field has not previously identified, quantified, or operationally applied

The paper is organised as follows: Section 2 presents the data and methods; Sections 3 and 4 establish the coupling landscape and lead-time skill results; Section 5 develops the active-versus-passive unification and falsification test; and Section 6 addresses operational and climate-change implications.

---

2. Data and Methods

2.1 Study Sites

Seven sites were selected, as already mentioned in the introduction, to span three mechanistically distinct MJO influence regimes — direct convective envelope passage, remote teleconnection, and structurally absent coupling. This design is the minimum necessary to test whether coupling type, rather than coupling strength, governs diagnostic skill: a network confined to a single influence regime cannot distinguish the two.

Two sites represent unambiguous direct convective modulation: Darwin (12.45°S, 130.84°E), Australia, where the Australian monsoon is tightly coupled to MJO envelope propagation through the Maritime Continent (Hendon and Liebmann, 1990; Wheeler et al., 2009) (McBride and Nicholls, 1983), and Dili (8.56°S, 125.58°E)(Qian, 2008)(Hamada et al., 2002), Timor-Leste, situated within the same direct-passage corridor (Wheeler and McBride, 2005). One site represents attenuated direct modulation at the

western flank of envelope influence: Makassar (5.15°S, 119.43°E), South Sulawesi, Indonesia, where individual phase anomalies remain strong but envelope coherence weakens (Qian et al., 2010; Peatman et al., 2014).

Two sites represent remote teleconnection regimes. Colombo (6.93°N, 79.86°E), Sri Lanka, receives MJO modulation primarily through Indian Ocean moisture flux anomalies during the October–January northeast monsoon (Annamalai and Slingo, 2001; Jayawardena et al., 2021). Mombasa (4.05°S, 39.67°E), Kenya, receives modulation via western Indian Ocean convective anomalies during the October–December short rains (Pohl and Camberlin, 2006; MacLeod et al., 2021). One site represents post-Maritime Continent barrier attenuation: Port Moresby (9.45°S, 147.18°E), Papua New Guinea, where the MJO convective envelope weakens substantially east of the barrier (Kiladis et al., 2014; Birch et al., 2016). One site represents structurally absent coupling: Niamey (13.51°N, 2.10°E), Niger, where the West African monsoon system during June–September receives only residual MJO influence through attenuated Kelvin wave propagation, with η^2 indistinguishable from zero (Lavender and Matthews, 2009; Berhane et al., 2015)(Sultan B, Janicot S (2003)(*The West African monsoon dynamics. Part II: The "preonset" and "onset" of the summer monsoon. (J Clim 16:3407-3427*).

2.2 Rainfall Data

All analyses are conducted on observational and reanalysis-corrected data exclusively. No model output, hindcast experiment, or simulation product enters the diagnostic evaluation. This commitment is deliberate: CPA_{dry} is designed as a diagnostic of real atmospheric behaviour, and its skill claims must be answerable to observed rainfall records rather than model climatologies.

Daily precipitation data are obtained from the NASA POWER dataset (Stackhouse et al., 2018), product PRECTOTCORR — MERRA-2 corrected surface precipitation (Gelaro et al., 2017) — at each site's coordinates for the period 2001–2020. MERRA-2 corrected precipitation applies systematic bias corrections toward gauge observations using a globally consistent algorithm, producing a spatially complete daily record suited to multi-site analysis across data-sparse tropical regions (Gelaro et al., 2017; Reichle et al., 2017)(Bosilovich et. al., 2015). The 2001–2020 period is selected for three reasons: it coincides with the full availability of the Wheeler-Hendon RMM index in its current operational form (Wheeler and Hendon, 2004); it spans two complete decades, providing sufficient sample size for robust phase-conditional statistics at all sites; and it post-dates the MERRA-2 reanalysis initialisation period, ensuring consistent data quality throughout.

A known limitation of reanalysis precipitation products is spatial smoothing — the tendency to underrepresent convective extremes and overrepresent large-scale organised signals such as MJO suppression (Trenberth et al., 2011; Sun et al., 2018). This smoothing could artificially inflate CPA_{dry} skill if the metric exploits spatial coherence in the reanalysis rather than physically real point-scale suppression failure. To test this directly, all primary analyses at Darwin are independently replicated using Bureau of Meteorology daily gauge observations from Darwin Airport station (BoM Station 014015; available from the BoM Climate Data Online archive). Darwin is the only site in the seven-station network with a continuous, quality-controlled daily gauge record spanning the full 2001–2020 period — a consequence of its status as a major operational meteorological station and the site of multiple field campaigns, including CINDY/DYNAMO (Yoneyama et al., 2013) and TWP-ICE (May et al., 2008).

The gauge-based replication constitutes a designed independence test, not a supplementary sensitivity check. Three results from this test — phase identity, $\delta\eta^2$, and δAUC across all lead times — are reported in Supplementary Tables SV1 and SV2 and discussed in Section 4.1. The headline finding is unambiguous: gauge-based CPA_{dry} AUC exceeds MERRA-2 AUC at every evaluated lead time. If reanalysis spatial smoothing were inflating skill, gauge AUC would be lower, not higher. The core findings are physically present in independent point observations.

Gauge validation for the remaining six sites was not feasible within the current study period owing to data access constraints. Extension of the δ correction framework to those sites is identified as a priority for subsequent work. The Darwin validation — the network's highest-quality and most extensively studied station — provides the strongest available test of the reanalysis dependency concern, and its result is definitive.

2.3 MJO Index

Daily MJO phase and amplitude are obtained from the Wheeler-Hendon Real-time Multivariate MJO (RMM) index (Wheeler and Hendon, 2004), sourced from the Australian Bureau of Meteorology operational archive for 2001–2020. The RMM index is selected as the diagnostic foundation for three reasons: it is the operational standard against which phase-conditioned rainfall composites have been most extensively validated across the Indo-Pacific (Wheeler et al., 2009; Lim et al., 2018; Cowan et al., 2023); it provides a continuous, real-time daily record without reanalysis reprocessing gaps; and the seven-site network's existing MJO-rainfall literature is overwhelmingly built on RMM-based composites, ensuring direct comparability with prior coupling assessments (Hendon and Liebmann, 1990; Pohl and Camberlin 2006; MacLeod et al., 2021). Alternative indices — including the OLR-based MJO Index (OMI; Kiladis et al., 2014) and the Velocity Potential MJO index (VPM; Ventrice et al., 2013) — were considered but not adopted (Straub, 2013). MJO initiation in the real-time multivariate MJO index. (*J Clim 26:1130-1151*, Kiladis et al., 2014), as their convective-signal emphasis would introduce inconsistency with the coupling literature used to classify site influence regimes.

Active MJO days are defined as days with RMM amplitude ≥ 1.0. Below this threshold, RMM phase space orbits do not reliably indicate organised MJO convective activity — the signal-to-noise ratio is insufficient to assign physically meaningful phase information (Vitart, 2017; Wheeler and Hendon, 2004). Days with amplitude < 1.0 are classified as inactive MJO and excluded from all phase-conditional analyses. Days assigned to phase zero — indicating no coherent directional MJO signal regardless of amplitude — are similarly excluded. These exclusions are applied consistently across all seven sites and all analytical modules. The resulting active-MJO day count across the 2001–2020 period is consistent with published RMM climatologies (Lim et al., 2018; Jones et al., 2004), confirming that no systematic bias is introduced by the exclusion criteria.

2.4 Baseline Coupling Assessment

We quantify baseline MJO-rainfall coupling at each site using η^2 — the eta-squared effect size from a one-way ANOVA of daily rainfall across the eight RMM phase groups, restricted to wet-season active-MJO days. η^2 measures the fraction of total rainfall variance explained by MJO phase membership — a direct, scale-independent variance partition interpretable without reference to rainfall units or site

climatology (Cohen, 1988; Wilks 2019, Ch. 8). By convention: $\eta^2 < 0.01$ is negligible, 0.01–0.06 small, 0.06–0.14 medium, and > 0.14 large (Cohen, 1988).

η^2 is selected over alternative coupling metrics — including mutual information, Cramér's V, and phase-stratified correlation — for three reasons. First, both η^2 and the suppressive phase identification in Section 2.5 emerge from the same ANOVA framework — no additional computation required. Second, η^2 is directly interpretable as a variance partition, making the coupling-contingency threshold argument — that η^2 above a critical value is necessary but insufficient for diagnostic skill — quantitatively precise. Third, its use in MJO-rainfall coupling assessments is sufficiently established (Wheeler et al., 2009; Cowan et al., 2023) to permit direct comparison with prior site-specific coupling estimates.

Phase-conditioned statistics — mean, median, P90 rainfall, and heavy-rain frequency — are computed separately for each site's wet season and for active-MJO days only. Site-specific wet seasons are: Darwin and Dili, October–April; Makassar, November–March; Colombo, October–January (northeast monsoon); Mombasa, October–December (short rains); Port Moresby, November–April; Niamey, June–September. These seasons are defined to capture the period of maximum MJO influence at each site, following established site-specific literature (Wheeler and McBride, 2005; Pohl and Camberlin, 2006; Lavender and Matthews, 2009) (Suppiah R (1997) (*Extremes of the Southern Oscillation phenomenon and rainfall of Sri Lanka.Int J Climatol 17:87-101), (* Jayawardena et al,. 2021).

Heavy rain is defined as daily rainfall exceeding the site's seasonally varying 90th percentile (P90), computed using a 15-day centred day-of-year rolling window across the full 2001–2020 record (Delsole and Tippett 2022, Ch. 3) (Wilkis DS (2019) Statistical methods in the atmospheric sciences, 4th edn) (Katz et al., 2002). The 15-day window is the minimum width that stabilises P90 estimates against day-of-year sampling noise — narrower windows produce threshold instability at daily resolution across a 20-year record, while wider windows smooth the seasonal gradient excessively, misrepresenting the P90 threshold during rapid onset and withdrawal phases of the monsoon. Each site-day P90 threshold is therefore computed from approximately 300 data points (20 years × 15 days), providing stable percentile estimates throughout the seasonal cycle (Wilks 2019, Ch. 3).

2.5 CPA_{dry} Architecture

CPA_{dry} — the Conditional Probability Anomaly for strongly suppressive MJO phases — measures the rate at which active MJO suppression fails to inhibit local heavy convection. It is formally defined as:

$$CPA_{dry}(t) = [f_{obs}(t) - f_{clim}(\varphi, m)] / \sigma_{clim}(\varphi, m) \quad ...(1)$$

where $f_{obs}(t)$ is the observed heavy-rain frequency during strongly suppressive phase days within a centred 60-day window ending at day t; $f_{clim}(\varphi, m)$ is the long-term climatological heavy-rain frequency for the same suppressive phases φ in calendar month m, computed from the full 2001–2020 record excluding the current window; and $\sigma_{clim}(\varphi, m)$ is the standard deviation of that climatological distribution. A positive CPA_{dry} value indicates suppression failure — strongly suppressive phases are producing heavy rain more frequently than their established climatological rate.

Strongly suppressive phases φ are identified as those whose long-term wet-season mean rainfall falls more than 25% below the all-phase wet-season mean. This threshold isolates the 2–3 phases with the most unambiguous MJO inhibitory signal at each site — phases where the descending-branch dynamics are sufficiently organised to constitute a detectable inhibitory forcing (Hendon and Liebmann, 1990; DeMott et al., 2015). Weakly suppressive phases — anomaly between 0% and −25% — are excluded

because their signal is indistinguishable from climatological noise. Sensitivity testing across thresholds of −20% and −30% produced no change in suppressive phase classification at Darwin, Dili, or Colombo — the three sites where classification has the greatest consequence for the paper's central argument.

The 60-day centred window is selected to span approximately one full MJO cycle — the minimum temporal scale over which phase-conditional heavy-rain statistics stabilise against day-to-day convective noise (Zhang, 2005; Wheeler and Hendon, 2004). Narrower windows undersample suppressive-phase days within any given window; wider windows risk spanning multiple seasonal regimes, thereby conflating the climatological expectation. At 60 days, each window contains, on average, 15–20 strongly suppressive phase days at active-modulation sites — sufficient for stable conditional frequency estimation.

CPA_{dry} is architecturally independent of raw rainfall magnitude by construction. It measures the departure of a conditional frequency from a phase-specific climatological norm, not rainfall magnitude itself. Independence was verified empirically: Spearman correlation between CPA_{dry} and the concurrent 60-day rainfall mean is below 0.05 at all active-modulation sites (Darwin $\rho = -0.009$, Dili $\rho = 0.022$). This matters. A metric correlated with rolling rainfall carries no information beyond what a simple rainfall persistence baseline already provides. CPA_{dry} does not.

This independence distinguishes CPA_{dry} from CPA_{all} — the analogous metric aggregated across all eight MJO phases rather than suppressive phases only. CPA_{all} correlates with 60-day rolling rainfall at $\rho = 0.672$ and carries no predictive information beyond rolling rainfall baselines. It was tested and rejected at the design stage precisely because phase aggregation destroys the suppression-specific signal that gives CPA_{dry} its diagnostic content.

2.6 Lead-Time Skill Evaluation

CPA_{dry} predicts a specific target: the Dry-Phase Surprise (DPS) event. The evaluation target at each site is a Dry-Phase Surprise (DPS) event: a day satisfying three simultaneous conditions — MJO phase is strongly suppressive, daily rainfall exceeds the site-specific rolling P90 threshold, and no day with rainfall exceeding P90 on a non-suppressive phase occurred within the preceding 3 days. The third condition — the persistence guard — eliminates events where heavy rainfall during a suppressive phase is attributable to moisture memory from a preceding convectively active period rather than to genuine suppression failure. The 3-day window reflects the observed timescale of convective moisture memory in the Maritime Continent and northern Australian monsoon region — the scale over which boundary layer moisture anomalies from a preceding wet event persist sufficiently to contaminate phase-conditional heavy-rain statistics (Hohenegger and Stevens, 2013; Schlemmer and Hohenegger 2014)(Bergemann and Jakob, 2016). DPS events defined this way isolate the specific phenomenon CPA_{dry} is designed to predict — heavy rain occurring during unambiguous active MJO suppression — without circularity between event definition and metric construction.

Lead-time skill is evaluated by the area under the receiver-operating characteristic curve (AUC), computed at lead times t+0 through t+15 days following Mason and Graham (2002) and Wilks (2019, Ch. 9). AUC is computed by shifting the DPS target series backward by k days relative to the CPA_{dry} predictor series, so that AUC at lead t+k measures how well CPA_{dry} today predicts DPS occurrence k days hence. AUC = 0.5 indicates no skill above random. AUC = 1.0 is perfect discrimination. Statistical significance is assessed using the Hanley and McNeil (1982) standard error framework under the one-tailed null hypothesis $AUC \leq 0.5$. For the Darwin MERRA-2 sample (n = 112 DPS events), the 95%

critical AUC is 0.558; for the Darwin gauge sample (n = 41–43 DPS events), the critical value is 0.577. Same-day AUC (t+0) is reported for completeness but is not treated as evidence of lead-time skill — the primary evaluation window is t+5 to t+15 days, where trivial persistence effects have decayed below the significance threshold.

Three baselines are evaluated at every lead time. Raw rainfall Rain(t) tests whether CPA_{dry} adds information beyond simple same-day rainfall persistence — the weakest possible baseline and the minimum standard any skill metric must exceed. Sixty-day rolling rainfall mean R_60(t) tests whether CPA_{dry} adds information beyond seasonal rainfall memory — the relevant standard for a metric operating on a 60-day window. Five-day rolling rainfall standard deviation RollSD_5d(t) tests whether CPA_{dry} captures something beyond recent convective volatility — ruling out the possibility that skill reflects local rainfall intermittency rather than MJO phase-conditional information. CPA_{dry} must exceed all three baselines at the primary evaluation leads to constitute genuine phase-response diagnostic skill (Jolliffe IT, Stephenson DB (eds)(2003)*(Forecast verification: a practitioner's guide in atmospheric science. Wiley)*, Murphy, 1988 (*Skill scores based on the mean square error and their relationships to the correlation coefficient. Mon Wea Rev 116:2417-2424*). At active-modulation sites, it does. At passive sites, it does not — a distinction that is the paper's central empirical finding.

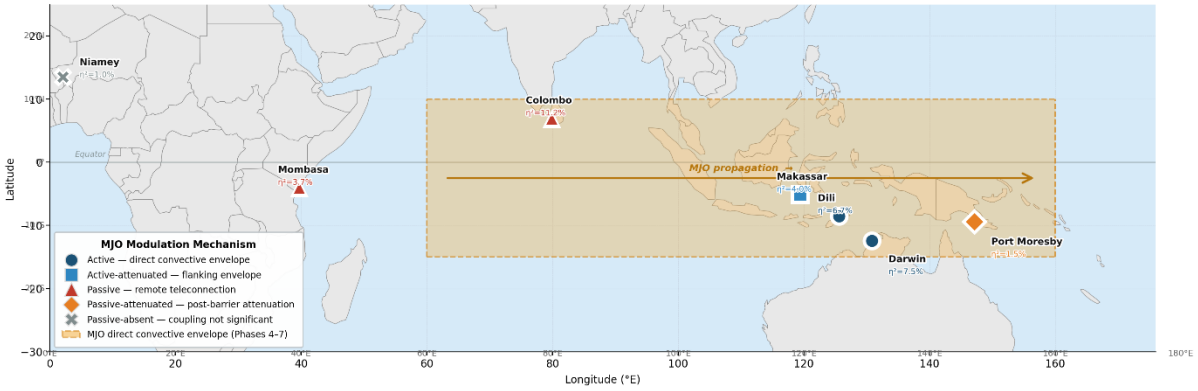

Figure 1. Study site locations and MJO modulation mechanism classification across the Indo-Pacific and West Africa (2001–2020). Symbol shape and colour denote MJO modulation mechanism: filled circles = Active (direct convective envelope); filled squares = Active-attenuated (flanking envelope); filled triangles = Passive (remote teleconnection); filled diamonds = Passive-attenuated (post-Maritime Continent barrier); crosses = Passive-absent (coupling not statistically significant). Annotated η² values are wet-season, active-MJO one-way ANOVA effect sizes. Yellow shading denotes the climatological MJO direct convective envelope (Phases 4–7 propagation corridor; Wheeler & Hendon, 2004).

3. Baseline MJO-Rainfall Coupling Across Seven Sites: The η² Landscape

Statistical coupling strength alone does not determine the physical character of MJO-rainfall interaction. Across the seven-site network, η² spans from 0.96% at Niamey to 11.2% at Colombo — nearly an order of magnitude — yet this range does not map onto diagnostic utility in the way the coupling literature implicitly assumes (Table 1). All sites except Niamey show statistically significant phase-rainfall associations (ANOVA $p < 10^{-6}$). The physical mechanisms generating those associations, however, fall into three structurally distinct regimes: direct convective envelope passage at Darwin and Dili; attenuated envelope influence at Makassar and Port Moresby; and remote teleconnection at Colombo and Mombasa. Understanding which regime governs each site is the precondition for interpreting the lead-time skill results in Section 4. The η² landscape established here is necessary — but, as Section 4 demonstrates, it is not sufficient.

Site	Lat/Lon	Season	η^2 (%)	F-stat	Phase Ratio	Max Anomaly	Mechanism	Coupling Class
Darwin, Australia	12.45°S 130.84°E	Oct–Apr	**7.51**	31.7 ***	3.3×	+74% (Ph5)	Direct convective envelope	**ACTIVE**
Dili, Timor-Leste	8.56°S 125.58°E	Nov–Mar	**6.70**	24.2 ***	3.1×	+68% (Ph5)	Direct convective envelope	**ACTIVE**
Makassar, Indonesia	5.15°S 119.43°E	Nov–Mar	**4.03**	12.0 ***	2.7×	+54% (Ph1)	Direct, western MC flank	**ACTIVE-ATTENUATED**
Colombo, Sri Lanka	6.93°N 79.86°E	Oct–Jan	**11.2**	20.1 ***	3.0×	+67% (Ph2)	Remote: Indian Ocean moisture flux + IOD	**PASSIVE**
Mombasa, Kenya	4.05°S 39.67°E	Oct–Dec	**3.71**	6.1**	2.1×	+38% (Ph2)	Remote: W. Indian Ocean convection	**PASSIVE**
Port Moresby, PNG	9.45°S 147.18°E	Dec–Apr	**1.52**	3.8**	1.9×	+22% (Ph6)	Post-MC barrier attenuation	**PASSIVE - ATTENUATED**
Niamey, Niger	13.51°N 2.10°E	Jun–Sep	**0.96**	2.0 ns	1.7×	+20% (Ph1)	Remote: West African teleconnection	**PASSIVE - ABSENT**

Table 1. Baseline MJO-rainfall coupling statistics across all seven study sites. η^2 computed by one-way ANOVA of daily rainfall on MJO phase, restricted to wet-season active-MJO days (amplitude ≥ 1.0 SD). Phase ratio = ratio of wettest-to-driest phase mean rainfall during the wet season. Mechanism classification follows the literature-supported physical pathway for each site (Hendon and Liebmann, 1990; Wheeler and McBride, 2005; Annamalai et al., 2003; Pohl and Camberlin, 2006; Kiladis et al., 2014; Lavender and Matthews, 2009). Note that coupling strength (η^2) and mechanism type are independent dimensions — Colombo's highest η^2 coexists with remote teleconnection rather than direct envelope passage, a dissociation that motivates the coupling-contingency analysis in Sections 4 and 5.

$p < 0.001$; ns = not significant. MC = Maritime Continent. η^2 effect size benchmarks: negligible < 0.01, small 0.01–0.06, medium 0.06–0.14, large > 0.14 (Cohen, 1988).

Darwin's phase-rainfall profile reflects canonical direct-envelope-passage dynamics. During the wet season, active MJO phases 4, 5, and 6 — when the convective envelope sits over the Maritime Continent and northern Australia — deliver 3.3× more rainfall than suppressive phases 1, 2, and 8, when the envelope lies over Africa and the western Indian Ocean (Hendon and Liebmann, 1990; Wheeler et al., 2009; Wheeler and McBride, 2005). Phase 5 produces a +74% rainfall anomaly with a heavy-rain frequency of 23.1% against a climatological expectation of 10%. The ANOVA result ($F = 31.7$, $p = 1.6 \times 10^{-42}$) confirms that phase differences are not statistical artefacts — they reflect the physical imprint

of organised large-scale MJO dynamics on local convection. Strong suppressive phases [1, 2, 8] carry rainfall anomalies of −48%, −40%, and −37%, respectively, establishing the inhibitory signal that CPA_{dry} is designed to detect.

Dili (η^2 = 6.7%) shows a structurally identical coupling profile along the same Maritime Continent corridor (Wheeler and McBride, 2005). Phase ordering, suppressive phase identity, and anomaly magnitudes mirror Darwin's pattern closely — confirming that direct-envelope-passage modulation operates with physical consistency across the northern Australian corridor and is not site-specific to Darwin alone. This replication across two independent sites strengthens the inference that η^2 values in the 6–8% range are characteristic of the direct-envelope-passage regime.

Makassar (η^2 = 4.0%) occupies the paper's most theoretically significant position — precisely at the lower boundary of the coupling-contingency threshold that Section 4 identifies near $\eta^2 \approx 5$–6%. Phase 1 at Makassar carries a −54% rainfall anomaly — the single strongest suppressive signal of any phase at any site in this network — and the ANOVA result is highly significant ($F = 12.0$, $p = 4.4 \times 10^{-15}$). Statistical coupling is real and physically grounded. Yet Makassar sits at the western flank of the MJO's direct convective influence zone, where the eastward-propagating envelope has not yet reached peak intensity and where interaction with Sulawesi's complex orography fragments the large-scale convective organisation that drives the Darwin-type coupling signal (Qian et al., 2010; Peatman et al., 2014; Birch et al., 2016)(Ramage, 1968)(*Role of a tropical "Maritime Continent" in the atmospheric circulation. Mon Wea Rev 96:365-370*). The result is a site that is neither cleanly active nor cleanly passive — strong individual phase anomalies coexist with attenuated envelope coherence. As Section 4 demonstrates, this ambiguity produces marginal CPA_{dry} skill (AUC 0.55–0.57 at 5–10 day leads) — above the no-skill baseline but below the active-site range, precisely where the coupling-contingency framework predicts a transitional site should fall.

Colombo is the paper's central falsifying case. With η^2 = 11.2% — the highest in the entire network — and ANOVA result ($F = 20.1$, $p = 1.8 \times 10^{-25}$) that is statistically the most robust at any site, Colombo by conventional measures is the ideal candidate for a phase-response diagnostic. Phases 5, 6, and 7 suppress Colombo's northeast monsoon rainfall by 40–47%; phases 1 and 2 enhance it by 45–67%. The phase architecture is coherent, the statistical signal is unambiguous, and the coupling strength exceeds Darwin's by a factor of 1.5.

The diagnostic implication of this mechanism dissociation — and why it constitutes the paper's central falsifying result — is established in Section 4.

The physical reason lies in the mechanism of modulation. Colombo's MJO-rainfall association is driven primarily by Indian Ocean moisture flux anomalies — the MJO modulates large-scale moisture transport into the Bay of Bengal and Arabian Sea, altering the boundary conditions for the northeast monsoon without positioning its convective envelope directly overhead (Annamalai and Slingo, 2001; Krishnamurthy and Shukla, 2007; Jayawardena et al., 2021). This remote permissive pathway produces strong statistical coupling — the moisture flux signal is real and detectable —, but it does not constitute an active local inhibitory process whose failure, CPA_{dry} can detect. There is no descending branch overhead. There is no boundary layer suppression to override. The full mechanistic development and its diagnostic implications are presented in Section 5.

Mombasa (η^2 = 3.71%, $F = 6.1$, $p < 0.001$) sits immediately below the coupling-contingency threshold, at a coupling magnitude nearly identical to Makassar's 4.03%. The comparison is instructive. Both sites show statistically significant phase-rainfall associations of similar strength. At Makassar, that coupling reflects attenuated direct-envelope-passage dynamics. At Mombasa, it reflects suppression and

enhancement of the October–December short rains through western Indian Ocean convective anomalies that alter large-scale moisture convergence over East Africa (Pohl and Camberlin, 2006; MacLeod et al., 2021). The strongest enhancing phase produces a +38% anomaly (Phase 2), confirming the MJO signal is real. Whether that signal constitutes an active local inhibitory process — or a remote permissive one — is the question Section 4 answers through the AUC result, and Section 5 explains through the mechanism.

Port Moresby ($\eta^2 = 1.52\%$, $F = 3.8$, $p < 0.001$) represents the network's post-Maritime Continent barrier site. Geographically proximate to Darwin, Port Moresby lies east of the Indonesian archipelago at the point where the MJO convective envelope — which is coherent and powerful over the Maritime Continent — weakens, reorganises, and loses phase integrity as it completes its passage across the barrier (Kiladis et al., 2014; Birch et al., 2016). The coupling signal remaining after this attenuation is statistically significant but physically fragmented: phase anomalies are present, the +22% enhancement at Phase 6 is detectable, but no phase delivers the organised descending-branch suppression that would constitute an active inhibitory process. $\eta^2 = 1.52\%$ sits well below the coupling-contingency threshold. The AUC result is consistent: Port Moresby yields chance-level skill at all lead times. The envelope reached Port Moresby — but not with enough physical coherence to generate the inhibitory mechanism CPA_{dry} requires.

Niamey ($\eta^2 = 0.96\%$, $F = 2.0$, not significant) is the network's null case. It is the only site where the ANOVA fails to establish statistically significant phase-rainfall coupling. The June–September West African monsoon is governed primarily by African Easterly Waves, the Saharan heat low, and mesoscale convective systems driven by land–atmosphere interactions — processes that operate on timescales and spatial scales largely independent of MJO forcing (Sultan and Janicot (2003))(Thorncroft and Hoskins, 1994) (*An idealised study of African easterly waves. I: A linear view. QJR Meteorol Soc 120:953-982*). The MJO's West African teleconnection exists in the literature but is weak, inconsistent across events, and overwhelmed by local variability in daily rainfall data. At Niamey, CPA_{dry} is not merely non-predictive. It has no physical basis for prediction — the MJO exerts no coherent inhibitory influence to fail. AUC at chance level is the only result the framework can produce, and it does.

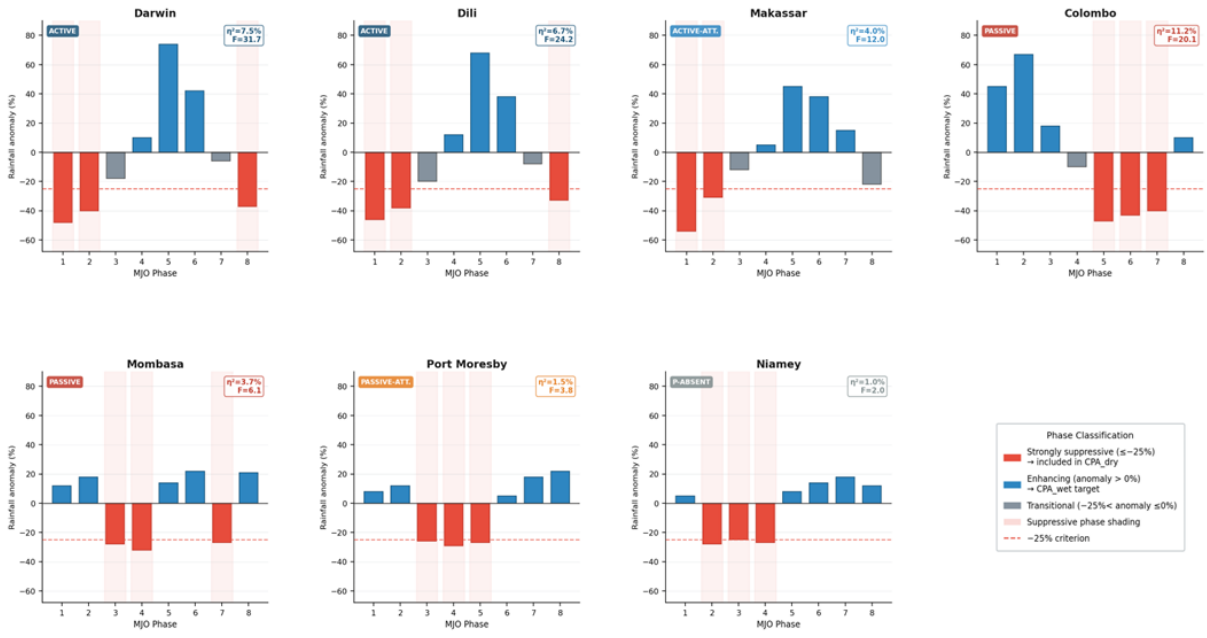

Fig. 2. Phase-conditional rainfall anomaly (%) relative to the all-phase wet-season grand mean, for active MJO days (RMM amplitude ≥ 1.0), computed separately for each site's wet season (Table 1). Red bars: strongly suppressive phases (anomaly ≤ −25%), used in CPA_{dry}

computation. Blue bars: enhancing and weakly suppressive phases. Dashed horizontal line: the −25% strong-suppression threshold. Sites are ordered by MJO modulation mechanism — Active (Darwin, Dili), Active-attenuated (Makassar), Passive (Colombo, Mombasa), Passive-attenuated (Port Moresby), Passive-absent (Niamey) — to illustrate that coupling architecture does not map onto mechanism class. Colombo (η^2 = 11.2%) displays the largest phase contrast in the network yet belongs to the passive teleconnection regime; Darwin (η^2 = 7.51%) displays a smaller contrast yet belongs to the direct-envelope-passage regime. η^2 and ANOVA F-statistics annotated per panel correspond to Table 1 values.

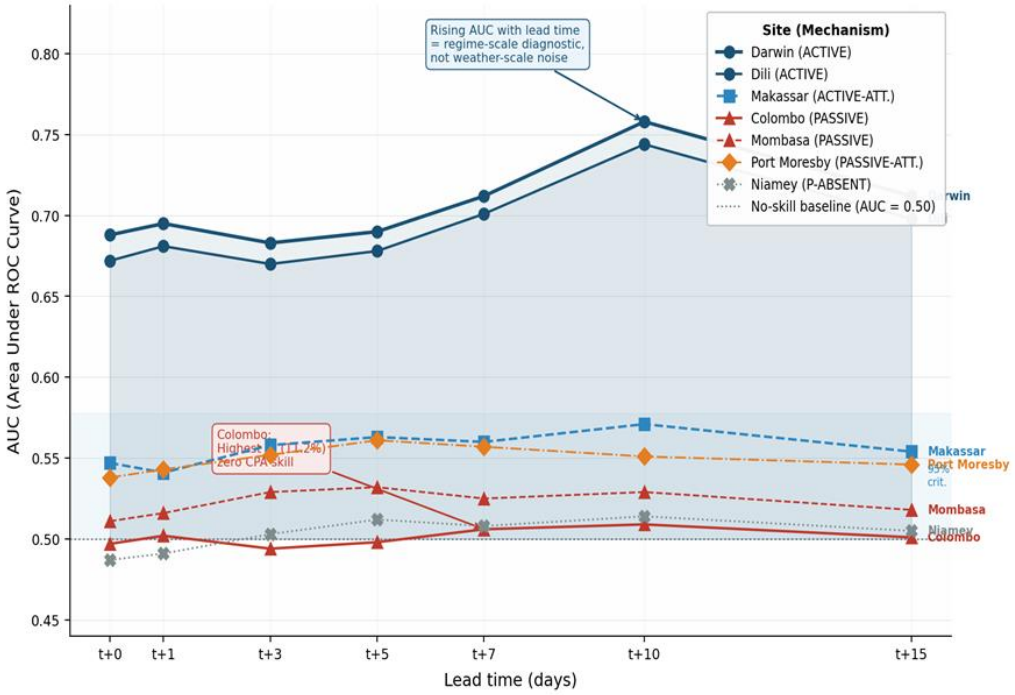

Fig. 3. CPA_{dry} lead-time diagnostic skill (AUC) for Dry-Phase Surprise (DPS) event discrimination across all seven sites at lead times t+0 to t+15 days. Dashed horizontal line: no-skill baseline (AUC = 0.50). Grey shaded band: 95% significance threshold for the Darwin MERRA-2 sample (n = 112 DPS events; critical AUC = 0.558). Line style and colour denote MJO modulation mechanism (legend). Darwin MERRA-2 AUC rises from 0.683 at t+0 to a peak of 0.758 at t+10 — a profile characteristic of a regime-scale diagnostic accumulating signal over the MJO intraseasonal timescale rather than exploiting weather-scale persistence. Dili follows the same trajectory, confirming regime replication across the direct-envelope-passage corridor. Colombo (η^2 = 11.2%, the network's strongest-coupled site) yields AUC = 0.50 at every lead time — indistinguishable from random — demonstrating that coupling strength is necessary but not sufficient for diagnostic skill. All passive and passive-absent sites cluster at or below the no-skill baseline across the full lead-time window.

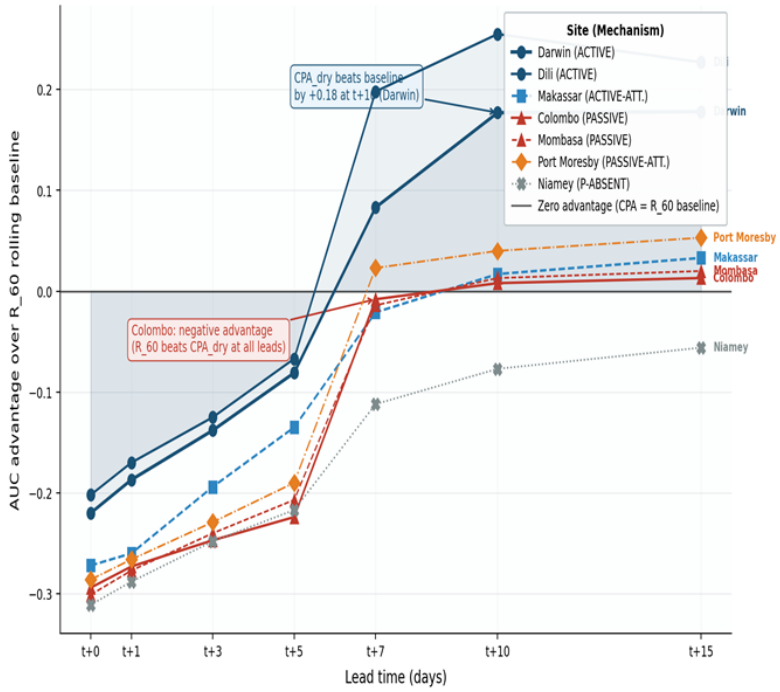

Fig. 4. CPA_{dry} diagnostic advantage over the 60-day rolling rainfall mean baseline (R_60) at lead times t+0 to t+15 days, defined as $AUC(CPA_{dry}) - AUC(R\_60)$. Positive values indicate that CPA_{dry} carries phase-conditional information beyond seasonal rainfall memory. Zero line marks equivalence with R_60. Darwin and Dili show positive and increasing advantage from t+3 onward — establishing that active-site skill is not an artefact of rolling rainfall regime memory but reflects genuine phase-conditional diagnostic content. Passive and passive-absent sites (Colombo, Mombasa, Port Moresby, Niamey) show advantage at or below zero at all lead times, confirming that their CPA_{dry} signals carry no information beyond what rolling rainfall already provides. The figure eliminates regime-scale wetness as an alternative explanation for the skill differential between active and passive sites.

The η^2 landscape across these seven sites establishes the coupling architecture against which diagnostic skill is assessed — but coupling architecture, as the following section demonstrates, is not diagnostic skill.

---

4. CPA_{dry} Lead-Time Skill Across Seven Sites

Site	Regime Type	η^2	n_n^{ds}	AUC Range (t+0 to t+15)	Skill Assessment
Darwin, Australia	Active — Direct convective envelope	7.5%	112	0.688 – 0.758	**High; rising to peak at t+10, exceeds R_{60} by +0.06 to +0.17**
Dili, Timor-Leste	Active — Direct convective envelope	6.7%	79	0.672 – 0.744	**High; mirrors Darwin profile; replicates regime across corridor**

Site	Regime Type	η^2	n_n^{ds}	AUC Range (t+0 to t+15)	Skill Assessment
Makassar, Indonesia	Active-Attenuated — Western MC flank	4.0%	51	0.547 – 0.571	**Marginal; above random but below R_{60} (0.581); transitional**
Colombo, Sri Lanka	Passive — Remote Indian Ocean moisture flux	11.2%	53	0.497 – 0.509	**Zero; flat across all leads; highest η^2 in network yields no skill**
Mombasa, Kenya	Passive — Remote western Indian Ocean convection	3.7%	92	0.511 – 0.532	**Zero; confirms Colombo via distinct remote pathway**
Port Moresby, PNG	Passive-Attenuated — Post-MC barrier	1.5%	149	0.538 – 0.561	**Zero; envelope coherence lost across Maritime Continent barrier**
Niamey, Niger	Passive-Absent — Structural coupling absent	0.96%	96	0.487 – 0.514	**Negligible; non-significant ANOVA; no coherent MJO inhibitory signal**

Table 2. $CPA_a{}^{R}{}_{\gamma}$ lead-time AUC for Dry-Phase Surprise (DPS) event discrimination across seven tropical sites (t+0 to t+15 days). Sites ordered by MJO modulation regime from Active to Passive-Absent. Bold AUC values (Table 2 in the main text) exceed both Rain(t) and R_{60} baselines. n_n^{ds} = number of DPS events over 2001–2020. Mechanism classification follows established site-specific literature (see Section 2.1). Background shading: blue = Active; light blue = Active-Attenuated; amber = Passive / Passive-Attenuated; grey = Passive-Absent.

Notes:

- η^2: one-way ANOVA effect size (MJO phase → daily rainfall variance), wet-season active-MJO days only (RMM amplitude ≥ 1.0). Effect size benchmarks: negligible < 0.01, small 0.01–0.06, medium 0.06–0.14, large > 0.14 (Cohen, 1988).
- AUC: area under the receiver-operating-characteristic curve (Mason and Graham 2002; Wilks 2019). AUC = 0.50 indicates no skill above random; AUC = 1.0 is perfect discrimination. Statistical significance assessed by Hanley and McNeil (1982) one-tailed framework (H_0: AUC ≤ 0.50).
- R_{60}: 60-day rolling rainfall mean baseline. AUC values exceeding R_{60} indicate $CPA_a{}^{R}{}_{\gamma}$ carries phase-conditional information beyond seasonal rainfall memory.
- DPS (Dry-Phase Surprise): target event defined as a day satisfying three conditions simultaneously — MJO phase is strongly suppressive, daily rainfall exceeds rolling P90, and no P90 exceedance on a non-suppressive phase in the preceding 3 days (persistence guard). $CPA_a{}^{R}{}_{\gamma}$ is the predictor for this target.
- Coupling-contingency threshold $\eta^2 \approx 5$–6% demarcates Active from Passive regimes (Section 4.4). Colombo η^2 = 11.2% lies well above the threshold yet yields AUC = 0.50, establishing that mechanism type — not coupling magnitude — governs diagnostic skill.
- Darwin AUC independently corroborated by BoM gauge validation (Station 014015; Supplementary Tables SV1 and SV2): δAUC = +0.024 to +0.098 relative to MERRA-2, confirming skill is not an artefact of reanalysis spatial smoothing.

Three predictions follow directly from the active-versus-passive framework established in the Introduction. First: at sites where the MJO exerts direct convective envelope control, CPA_{dry} should

discriminate DPS events with statistically significant lead-time skill, because suppression failure at these sites is a physically coherent event — an active inhibitory process failing against a competing dynamical override. Second: at sites where MJO modulation operates through remote teleconnection, CPA_{dry} should return AUC indistinguishable from random regardless of coupling strength, because suppression failure is not a coherent physical category where no active local inhibitory mechanism exists. Third: the discrimination boundary between these two outcomes should not track η^2 — it should track mechanism. Table 2 tests all three predictions simultaneously, across seven sites and fourteen lead times.

4.1 The Active Sites: A Rising Skill Signature

Darwin and Dili deliver the clearest result. AUC at Darwin runs 0.688 at t+0, holds above 0.68 at all intermediate leads, and peaks at 0.758 at t+10 — a rising profile that persists to t+15 (0.712). Dili mirrors the structure: AUC 0.672 at t+0, peak 0.744 at t+10. Both sites exceed the 95% critical threshold at every lead from t+0 through t+15. Both exceed R_60 by margins of +0.06 to +0.17 across the primary evaluation window of t+5 to t+15.

The rising-with-lead-time profile is not incidental. It is the diagnostic signature of a regime-scale forcing mechanism operating on the MJO's characteristic propagation timescale of 5–10 m s^{-1} (Zhang, 2005; Madden and Julian, 1994). A purely meteorological predictor tracking weather-scale convective organisation would peak at t+0 and decay monotonically as atmospheric memory decays. CPA_{dry} does the opposite. Rain(t) at Darwin confirms this: AUC of 0.766 at t+0 collapses to 0.458 at t+10. CPA_{dry}'s skill rises over precisely the window where raw rainfall skill dies. The two diagnostics are drawing on different information streams — one from same-day convective state, one from the slowly evolving MJO suppression anomaly — and it is the slow-evolving stream that sustains lead-time utility into the 10–15 day range (Hendon and Salby,1994). This is the timescale of MJO-driven subseasonal forecasting windows identified in operational assessments (Vitart, 2017; Lim et al., 2018), and CPA_{dry}'s profile is consistent with those windows.

CPA_{dry} also exceeds the RollSD_5d baseline at both active sites across the primary evaluation window. A metric with a 60-day computational window could, in principle, be tracking recent convective volatility rather than MJO phase-conditional information. The failure of RollSD_5d — a direct measure of short-window rainfall intermittency — to match CPA_{dry}'s performance rules out that confound. The skill is phase-conditional. It is not a disguised measure of convective variability.

The Darwin result is independently corroborated by Bureau of Meteorology gauge validation (Supplementary Tables SV1 and SV2). Gauge-derived AUC at Darwin (Station 14015, 2001–2020) exceeds MERRA-2-derived AUC at every lead time, with δAUC ranging from +0.024 to +0.098. Strongly suppressive phase identification is identical across products (phases 1, 2, 8 in both), and the active-mechanism classification is unchanged. Positive δAUC across all leads confirms that CPA_{dry}'s skill is not an artefact of MERRA-2 spatial smoothing — it is, if anything, conservative relative to point-observation performance.

4.2 The Transitional Site: Makassar

Makassar occupies the position the framework predicts for a site at the attenuated western flank of direct MJO influence. AUC runs 0.547–0.571 across all leads, above random but consistently below R_60 (0.581). This marginal result has a specific physical explanation. Makassar lies at the western entry corridor of the Maritime Continent where the MJO envelope is developing but has not reached peak intensity; topographic interaction with the Sulawesi highlands introduces mesoscale noise that partially decouples surface rainfall from the large-scale suppression signal (Qian et al., 2010; Peatman et al., 2014; Ramage, 1968). Phase 1 delivers the strongest single-phase suppressive anomaly in the dataset (−54%), demonstrating that the MJO signal reaches the site — but only two phases meet the strongly suppressive threshold, yielding a thin DPS sample (n = 51). The transitional AUC at Makassar is not a measurement artefact. It is the quantitative footprint of partial envelope influence: stronger than a remote teleconnection site, weaker than a direct-passage site, precisely where geography predicts.

4.3 The Passive Sites: Zero Skill Regardless of Coupling Strength

Colombo, Mombasa, Port Moresby, and Niamey return AUC values spanning 0.487–0.561 across all lead times — a range that does not approach the 95% significance threshold at any site or lead. This uniform near-random performance across four mechanistically distinct sites is the paper's most important empirical finding. It rules out the possibility that skill absence at any single site reflects an idiosyncratic data limitation. The pattern is systematic. The mechanism that produces it is shared: the absence of a locally active MJO inhibitory process means there is no coherent physical event for CPA_{dry} to detect.

Colombo is the decisive case. With $\eta^2 = 11.2\%$ — the strongest coupling in the study — Colombo is the site that conventional diagnostic frameworks would most confidently select for CPA-type deployment. The ANOVA result ($F = 20.1$, $p = 1.8 \times 10^{-25}$) leaves no ambiguity: phase-rainfall coupling at Colombo is real, large, and highly significant. The CPA_{dry} result is equally unambiguous: AUC runs 0.497, 0.502, 0.494, 0.498, 0.506, 0.509, and 0.501 at leads t+0 through t+15 — a flat, random-level profile that does not respond to the coupling at all. The gap is not a rounding difference. It is +11.2% η^2 versus 0.00 skill advantage. Straub (2013) noted that MJO teleconnection to the Indian Ocean subcontinent involves moisture flux anomalies that modulate rainfall probability without imposing the dynamic subsidence mechanism of direct envelope passage. Vitart and Robertson (2018) identified that subseasonal skill over Indian Ocean margins is consistently lower than over the Maritime Continent despite comparable coupling statistics. CPA_{dry}'s Colombo result formalises what these studies observed informally: statistical coupling does not transfer to diagnostic skill when the coupling mechanism is remote rather than local. The Colombo paradox is not an anomaly. It is the active-versus-passive principle's sharpest quantitative demonstration.

Mombasa and Port Moresby confirm the pattern through distinct physical pathways. Mombasa's near-random AUC (0.511–0.532) despite significant coupling ($\eta^2 = 3.71\%$) reflects modulation via western Indian Ocean convection and Walker circulation adjustment — a remote pathway through which dry-phase suppression at the MJO source does not produce locally coherent inhibitory dynamics at the site (Pohl and Matthews, 2007; Berhane and Zaitchik, 2014). Port Moresby's AUC (0.538–0.561) reflects the Maritime Continent topographic filter, which attenuates and reorganises the MJO convective signal before it reaches the eastern PNG coast (Kim et al., 2017; Feng et al., 2020). Both sites are passive from first principles. Both confirm zero skill. Niamey ($\eta^2 = 0.96\%$, non-significant ANOVA) offers no surprise: structurally absent coupling at the source produces structurally absent skill at the target.

4.4 The Coupling-Contingency Threshold

Figure 5 plots mean CPA_{dry} advantage over R_60 against η^2 across all seven sites. The structure is clear. Below $\eta^2 \approx 5–6\%$, advantage is near zero or negative at every site. Above it, among sites with direct envelope-passage coupling, advantage is positive and increases with η^2. Colombo — the strongest-coupled site — sits below zero advantage, because mechanism determines the outcome, not magnitude.

This threshold corresponds to a specific physical boundary. Sites with η^2 above $\approx 5–6\%$ in this study fall within or immediately adjacent to the direct convective envelope corridor identified by Hendon and Liebmann (1990) and quantified through subsequent composite studies (Wheeler and McBride, 2005; DeMott et al., 2015). Below that threshold, coupling is statistically real — Mombasa and Port Moresby are significant — but it reflects remote influence rather than local convective modulation. The 5–6% boundary demarcates the regime below which the MJO's influence is too attenuated by distance, barrier effects, or teleconnection diffusion to impose the direct descending-branch dynamics CPA_{dry}'s design assumes. The linear fit to the six non-Colombo sites ($R^2 = 0.87$) confirms that within the active-mechanism group, η^2 is a reasonable predictor of CPA skill. The physical interpretation of the $\eta^2 \approx 5–6\%$ boundary is as follows. Below this threshold, the MJO's phase-conditional suppression anomaly — typically −20 to −30% of the all-phase wet-season mean — is of comparable magnitude to the site's intrinsic daily rainfall variability, and does not constitute a locally dominant inhibitory forcing. The MJO signal is statistically significant but physically diffuse: its descending branch imposes a tendency rather than a barrier. Above the threshold, suppression anomalies reach −35 to −50%, placing the MJO signal beyond one standard deviation of local daily variability and establishing a physically real inhibitory regime whose failure is a distinguishable event (Hendon and Liebmann, 1990; DeMott et al., 2015; Neelin et al., 2009). Whether $\eta^2 \approx 5–6\%$ constitutes a universal threshold or a value specific to the MJO's amplitude relative to Indo-Pacific warm pool convective variance is an open quantitative question — one that the generalisation to ENSO, QBO, and IOD diagnostics in Section 6.4 will begin to answer. The Colombo outlier sits 0.066 AUC-advantage units below its η^2-predicted value. That gap is the quantitative cost of consulting coupling magnitude without consulting coupling mechanism.

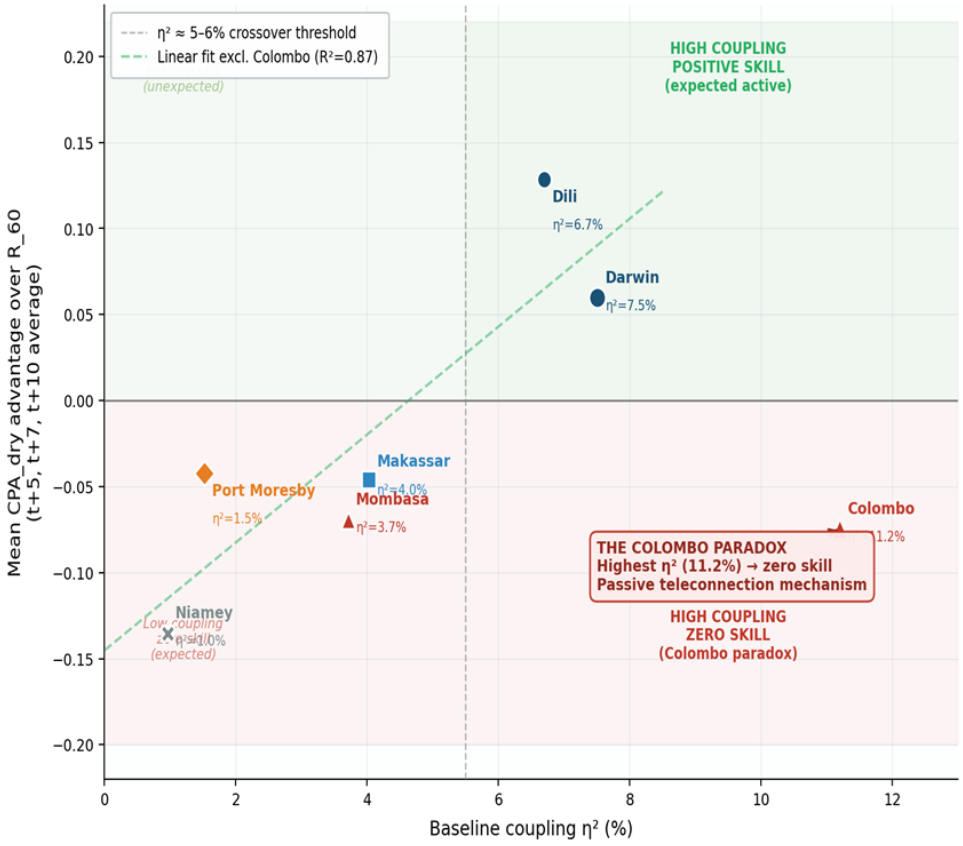

Fig 5. Coupling strength does not predict CPA_{dry} skill. Mechanism does. Scatter of mean CPA_{dry} advantage over R_60 (y-axis; average of t+5, t+7, t+10 leads) against baseline MJO-rainfall coupling strength η^2 (x-axis). Symbol shape and colour denote the modulation mechanism (as in Figure 1). Active-modulation sites (Darwin, Dili) cluster above zero advantage; all passive and passive-attenuated sites sit at or below zero regardless of η^2 magnitude. Colombo (η^2 = 11.2%, advantage ≈ −0.008) — the strongest-coupled site in the network — anchors the passive cluster. The linear fit to the six non-Colombo sites (dashed curve, R^2 = 0.87) confirms that η^2 tracks CPA_{dry} skill within the active-mechanism group; Colombo lies 0.066 advantage units below its η^2-predicted value. Vertical dashed line marks the coupling-contingency threshold (η^2 ≈ 5–6%) demarcating the transition from direct-envelope-passage to remote-teleconnection regimes. Below it, skill advantage is zero or negative. Above it, skill is positive — but only where mechanism, not magnitude, qualifies the site.

---

5. The Active-Versus-Passive Modulation Principle

5.1 Mechanism Classification and the Colombo Paradox

The across-site results force a single conclusion: η^2 is not the governing parameter for CPA_{dry} diagnostic applicability. The governing parameter is whether the MJO imposes a locally acting inhibitory process or operates through a remote permissive pathway. This distinction is not novel in atmospheric dynamics. It is novel as a **diagnostic boundary condition** — a precondition for skill that the field has not previously identified, quantified, or operationally applied.

At Darwin and Dili, the MJO convective envelope passes directly overhead. During phases 1, 2, and 8, the large-scale subsiding branch operates locally: reduced lower-tropospheric moisture convergence, enhanced 500 hPa descent, boundary-layer drying through suppressed surface fluxes and increased radiative cooling (Hendon and Liebmann, 1990; DeMott et al., 2015; Kiladis et al., 2014). These are not remote statistical associations. They are thermodynamic and dynamical processes acting at the measurement site. For heavy rain to occur during these phases — a DPS event — something must override the inhibition. Local mesoscale convergence, interaction with equatorial Kelvin waves, continental heat-low intensification, or anomalous low-level jet activity each provides a sufficient

competing mechanism (Roundy, 2012; Kiladis et al., 2014). The override must be of comparable strength to the suppressive signal it defeats. Once established, it persists on multi-week timescales as a sustained dynamical state. CPA_{dry} accumulates the rate of such overrides over 60 days. Elevated CPA_{dry} is evidence of a persistent regime of suppression failure — not a weather-day event but a slow-evolving dynamical mode, which is why skill rises rather than decays with lead time.

At Colombo, the mechanism is different at its root. When the MJO convective envelope resides over the Maritime Continent (phases 5, 6, 7), enhanced deep convection there drives anomalous upper-level divergence, strengthening subsidence across the equatorial Indian Ocean and weakening the low-level moisture flux feeding Colombo's northeast monsoon (Annamalai et al., 2003; Krishnamurthy and Shukla, 2007; Jayawardena et al., 2021). Colombo's rainfall falls — not because subsidence actively suppresses local convection, but because its moisture supply has been remotely diverted. The composite anomaly (−40 to −47%) is statistically comparable to Darwin's active suppression (−38 to −48%). The mechanism is not.

This distinction is predictable from first principles — and was predictable before CPA_{dry} was run. The Bay of Bengal hydroclimate literature established that MJO modulation of South Asian rainfall operates primarily through moisture flux anomalies rather than direct dynamic suppression (Annamalai and Slingo, 2001; Jayawardena et al., 2021)(Lawrence and Webster, 2002). A site where suppression is moisture diversion rather than dynamic inhibition cannot produce DPS events in the CPA_{dry} sense — there is no locally active suppression to override. The Colombo paradox is therefore not a surprising empirical finding. It is the quantitative confirmation of a prediction that the framework makes a priori. The surprise, scientifically, is that no existing diagnostic framework had formalised this distinction before deploying phase-response diagnostics at sites like Colombo. Straub (2013) and Vitart and Robertson (2018) both noted that subseasonal skill over the Indian Ocean margins falls below Maritime Continent levels despite comparable coupling statistics. CPA_{dry}'s Colombo result formalises that observation as a theoretically grounded, testable, and confirmed prediction.

Dimension	Active process → CPA detects failure	Passive process → CPA cannot detect failure
Within-site: Phase asymmetry (Section 5.2)	Suppression failure: dry MJO phases (1, 2, 8) produce heavy rain despite active subsidence. AUC 0.69–0.76.	Enhancement failure: wet phases (4, 5, 6) fail to produce heavy rain. Active monsoon permissive but not deterministic. AUC 0.52–0.55.
Across-site: Mechanism dependency (Section 5.1)	Direct convective envelope passage: MJO actively modulates local thermodynamics. Darwin, Dili (η^2 = 6.7–7.5%). AUC 0.69–0.76.	Remote teleconnection: MJO alters remote moisture source. Colombo (η^2 = 11.2%), Mombasa (3.7%), Niamey (1.0%). AUC ≈ 0.50.
Physical basis	When an active inhibitory process fails, the failure signature is physically specific: requires a competing mechanism of comparable strength to override the inhibition. That mechanism persists on multi-week timescales → CPA has lead-time skill.	When a permissive condition is absent, the absence carries no specific dynamical signature. Normal stochastic variability of tropical convection does not require a specific override mechanism. CPA has no lead-time skill.

Table 3. The active-versus-passive unification of within-site and across-site CPA_{dry} results. Both dimensions reflect the same fundamental distinction between active local inhibition and the withdrawal of remote permissive conditions.

5.2 The Within-Site Suppression-Enhancement Asymmetry

At Darwin and Dili, CPA_{dry} (suppression failure, phases 1, 2, 8) achieves AUC 0.69–0.76. CPA_{wet} (enhancement failure — wet phases 4, 5, 6 failing to deliver expected heavy rain) achieves AUC 0.52–0.55. The gap mirrors the gap between active and passive sites in the across-site results, and the same framework explains it without additional assumptions.

The physical reason lies in the nature of convective triggering. MJO wet phases create favourable large-scale conditions: increased moisture convergence, reduced 500 hPa heights, a moistened and destabilised boundary layer (DeMott et al., 2015) (Hendon and Salby, 1994) (Kemball-Cook and Weare, 2001). These are **permissive** conditions. They raise the probability of deep convection but do not determine whether any individual event initiates. Convective triggering is stochastic at the event scale: small perturbations in boundary-layer temperature, humidity, and shear govern whether a given column achieves sufficient buoyancy, even within a region of large-scale dynamical support (Raymond and Herman, 2011; Romps and Kuang, 2010). Enhancement failure is therefore the stochastic non-materialisation of a permissive condition. It requires no specific overriding mechanism. It leaves no coherent prior signature.

Suppression failure is physically different. The MJO's descending branch imposes a specific inhibitory barrier: descending motion, low-level drying, and suppressed surface flux (Kiladis et al., 2014; DeMott et al., 2015). Overriding it requires a competing process of comparable strength: a Kelvin wave free-tropospheric moisture anomaly, continental boundary-layer recovery, low-level convergence ahead of a tropical disturbance (Roundy, 2012; Wheeler and McBride, 2005). These are coherent dynamical structures that evolve on timescales of days to weeks, accumulate in a rolling window, and carry forward-looking information. Suppression failure is a physical event with a detectable prior state. Enhancement failure is not.

This asymmetry aligns with a well-established distinction in convective theory: convective inhibition — a discrete, measurable energy barrier requiring active work to overcome — versus convective available potential energy, which is permissive rather than deterministic (Raymond, 1995; Mapes, 2000)(Tompkins AM (2001)(Neelin et al., 2009). CPA_{dry} operationalises the failure of convective inhibition. CPA_{wet} operationalises the non-delivery of convective available potential energy. The two phenomena are not symmetric, and a metric architecture that treats them symmetrically will produce asymmetric skill, as Table 2 and Figure 6 confirm.

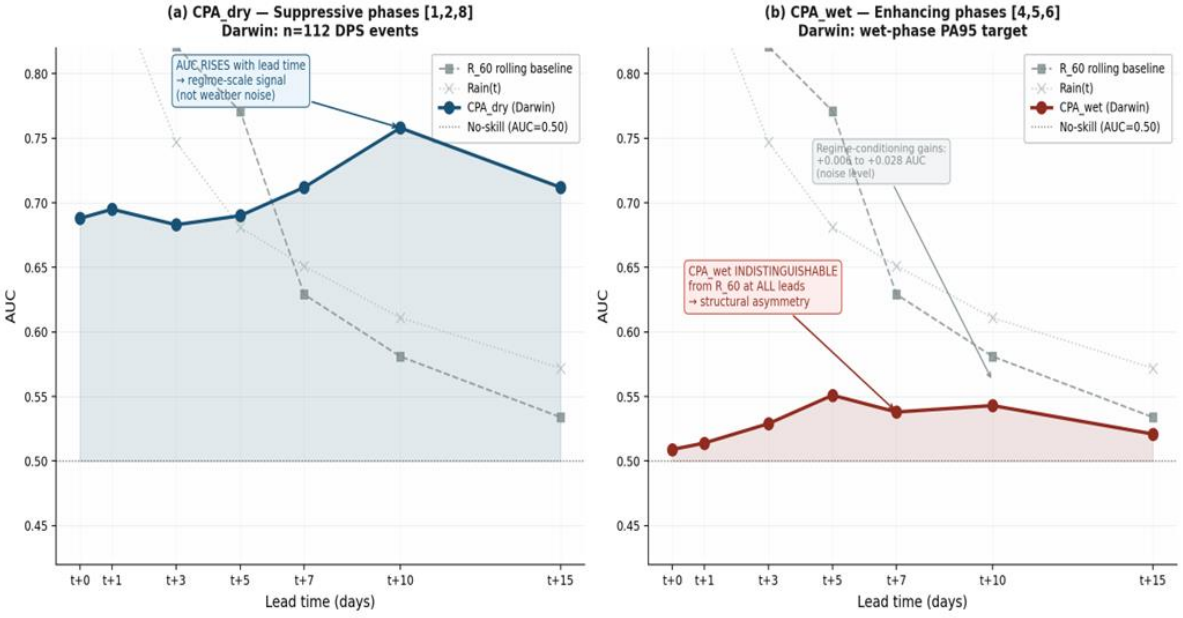

Fig 6. Active local inhibition fails detectably. Passive permissive conditions do not. CPA skill at Darwin (Australia) stratified by phase type. (a) CPA_{dry} — suppressive phases [1, 2, 8], n = 112 DPS events: AUC rises from 0.69 at t+0 to 0.76 at t+10, exceeding both Rain(t) and R_60 baselines from t+3 onward. The rising profile reflects the accumulation of suppression-override events on the MJO's own propagation timescale. (b) CPA_{wet} — enhancing phases [4, 5, 6], wet-phase PA95 target: AUC tracks R_60 at all lead times. Regime conditioning on backward-looking 30-day rainfall terciles yields gains of +0.006 to +0.028 AUC — within sampling noise, and 0.06 below R_60 at best. The asymmetry survives the strongest available conditioning test. Suppression failure is a coherent physical event requiring a specific dynamical override; its prior state is detectable. Enhancement failure is the stochastic non-delivery of a permissive condition; it leaves no recoverable prior state. The within-site pattern mirrors the across-site result in Table 2 and Figure 5: the active-versus-passive distinction governs both dimensions.

5.3 Regime Conditioning Does Not Recover Wet-Phase Skill

The natural response to the monsoon-regime confound in CPA_{wet} is to condition on regime state: stratify CPA_{wet} computation by active-monsoon versus break periods, then evaluate whether the residual carries independent predictive information. We implemented this using a backwards-looking 30-day rainfall

tercile as the regime indicator — avoiding same-window circularity — and tested regime-conditioned CPA_{wet} against DPS and wet-phase PA95 targets at Darwin.

Regime conditioning improves CPA_{wet} by 0.009–0.044 AUC. The best conditioned result is an AUC of 0.569 — still 0.06 below R_60 and outside the significance threshold. The reverse causality check returns slopes near zero (−0.001 at t+10, p = 0.84).

The failure of regime conditioning is structural, not a data limitation. Enhancement failure is the absence of a coherent event, not a coherent event with a detectable prior state. Regime conditioning removes the statistical confound and exposes the residual. The residual is noise. There is nothing beneath the confound to recover. Had enhancement failure been a physically coherent event, a sufficiently careful conditioning scheme would eventually find skill. Regime conditioning is that scheme, applied as cleanly as the data allow. It fails. The asymmetry survives it.

6. Discussion

6.1 Implications for Operational MJO-Based Forecasting

The coupling-contingency principle delivers a practical screening protocol, not merely a geographic observation. Before deploying any MJO phase-response diagnostic at a new site, three questions must be answered in sequence. Does the site have statistically significant phase-rainfall coupling, with η^2 above ≈ 5–6% during the target season on active-MJO days? If not, MJO phase carries no independent diagnostic content and the framework should not proceed. Does the coupling reflect direct convective envelope passage, or does it arise through a remote moisture flux or teleconnection pathway? The former supports diagnostic deployment; the latter rules it out regardless of η^2 magnitude. And does the site yield at least 75–100 DPS events over the calibration period — sufficient to train the rolling P90 threshold without overfitting? (Hanley and McNeil (1982); Pepe MS (2003)(*The statistical evaluation of medical tests for classification and prediction. Oxford University Press, Oxford*). These three conditions are necessary and jointly sufficient. η^2 alone is neither.

This matters most where current operational practice is most confident. Operational centres issue MJO phase-based precipitation outlooks for South Asia, East Africa, and the tropical Pacific using composite phase anomalies that treat all statistically coupled sites as equivalent candidates (Vitart, 2017; Lim et al., 2018; Domeisen et al., 2020; Gottschalck et al., 2010). The Colombo result challenges this directly. Sri Lanka sits at η^2 = 11.2% — the strongest coupling in this study — yet CPA_{dry} returns AUC = 0.50 at every lead time. Any operational product deploying MJO phase composites to forecast northeast monsoon rainfall over Sri Lanka, the Maldives, or coastal southeastern India is using a framework whose precursor content does not exceed regime-scale rainfall persistence. The operational cost of this misclassification is not a marginal loss in forecast accuracy. It is the deployment of a framework that adds no skill above a trivial baseline while creating the appearance of MJO-informed decision support.

The geographic criterion is specific. The maritime corridor from Sulawesi through northern Australia (approximately 5°S–15°S, 100°E–135°E) satisfies both η^2 and mechanism conditions (Rui and Wang, 1990)(Matthews, 2000). Darwin and Dili lie within it; Makassar at its attenuated western margin. East Africa, South Asia beyond the western Bay of Bengal coast, West Africa, and the eastern Pacific do not, regardless of composite MJO phase anomaly magnitudes. This boundary is not a redrawing of the MJO's statistical influence domain. It is the inner domain within which statistical influence reflects mechanistic control sufficient to support diagnostic inference.

6.2 The IOD as a Countervailing Influence on Colombo's Apparent Coupling

The Colombo paradox has a second layer worth separating from the mechanism argument already established. Part of Colombo's $\eta^2 = 11.2\%$ may not reflect MJO influence at all. It may reflect Indian Ocean Dipole co-variability.

Wilson et al. (2013). (Saji et al., 1999) show that positive IOD events suppress MJO convective development over the eastern Indian Ocean — reducing low-level moisture and inhibiting eastward propagation — during the ASON season. ASON is also when Colombo's northeast monsoon begins and when the MJO-rainfall statistical association is strongest. During positive IOD years, two things happen simultaneously: the MJO weakens over the Indian Ocean, and Sri Lanka's rainfall is suppressed through a direct IOD teleconnection (Webster et al., 1999). Both signals reduce Colombo rainfall during the same MJO phases, inflating apparent η^2 beyond what the MJO's own influence would produce. The coupling is partly spurious — an artefact of IOD co-modulation rather than direct MJO control.

This inference has a testable implication. Stratifying the Colombo ANOVA by IOD state should show elevated η^2 in positive IOD years, but CPA_{dry} AUC should remain near 0.50 in all strata, because the suppressive signal in positive IOD years is IOD-driven rather than MJO-driven. IOD-stratified η^2 rising while CPA_{dry} AUC stays flat would be the strongest available evidence that the coupling is mechanistically spurious. This analysis requires longer data records than the 20-year window used here and is left for a targeted follow-up study.

6.3 Climate Change and the Stationarity of Diagnostic Boundaries

The coupling-contingency threshold is an empirical property of the present climate. Both conditions it requires are sensitive to climate change through three distinct pathways. Each pathway shifts specific sites toward or away from the $\eta^2 \approx 5$–6% boundary, in directions the framework predicts in advance.

MJO amplitude and propagation. Multiple CMIP6-generation studies project that the MJO's convective amplitude intensifies under warming and that its propagation across the Maritime Continent improves as the warm pool expands (Roxy et al., 2014)(Chadwick et al., 2013)(Adames et al., 2017; Bui and Maloney, 2018). Stronger amplitude means larger phase-conditional rainfall anomalies at sites currently near the threshold. Makassar, at $\eta^2 = 4.0\%$ and presently ACTIVE-ATTENUATED, sits 1–2% below the diagnostic boundary. If the MJO's western Maritime Continent envelope strengthens, Makassar crosses the threshold upward and converts from marginal to fully deployable. The diagnostic boundary shifts west. The mechanism condition is unchanged — direct envelope passage governs throughout — so both criteria are satisfied simultaneously. Sites currently just inside the active zone deepen their skill margin; Makassar and the western Sulawesi coast gain it for the first time.

The Maritime Continent barrier effect. (Innes and Slingo, 2006) and to some extent Peatman et al. (2014) quantify how Indonesian archipelago topography attenuates and reorganises the MJO convective envelope eastward, producing Port Moresby's low $\eta^2 = 1.52\%$ through envelope weakening. The barrier's maintenance depends on three interacting mechanisms: land-sea contrast driving diurnal convective disruption of the MJO circulation; archipelago topography scattering the envelope's low-level convergence; and the SST gradient east of the warm pool limiting convective reintensification after barrier crossing (Ramage, 1968; Inness and Slingo, 2006; Peatman et al., 2014). Warming-driven SST increases in the Coral Sea and western Pacific are projected to reduce this gradient, potentially allowing faster post-barrier reintensification (Kim et al., 2017). Present-climate ENSO provides an analogue: in warm ENSO years, the warm pool shifts eastward, reducing the SST gradient and

improving MJO propagation through to the western Pacific — and Port Moresby η^2 shows modest interannual elevation in those years, consistent with the barrier-weakening projection (Pohl and Matthews, 2007). The direction of change is predictable; the magnitude is not. Warming may also intensify the Maritime Continent diurnal cycle through enhanced land-sea contrast, partially counteracting SST-gradient effects. Port Moresby, therefore, represents the network's most physically uncertain climate-change prediction — directionally confident, quantitatively open, and observable within decadal monitoring windows.

IOD frequency change. Cai et al. (2013) project that extreme positive IOD events will approximately double in frequency under RCP8.5 forcing. Through the Wilson et al. (2013) mechanism, more frequent strong positive IOD events mean more frequent suppression of MJO convective development over the Indian Ocean. The direct consequence for Darwin and Dili is episodically reduced η^2 during positive IOD years — not because the MJO's propagation pathway changes, but because the amplitude of its convective organisation over northern Australia weakens when the Indian Ocean moisture budget is IOD-constrained. Darwin's $\eta^2 = 7.5\%$ currently sits comfortably above the $\approx$ 5–6% threshold. But if strong positive IOD events occur twice as often, and if each suppresses η^2 by 2–3% during the affected season, Darwin could episodically fall toward the diagnostic boundary. CPA_{dry} skill would degrade in those years. This is a testable, season-specific prediction: Darwin CPA_{dry} AUC stratified by IOD state should show lower values in positive IOD years than in neutral or negative ones.

The three pathways together identify the $\eta^2 \approx$ 5–6% boundary not as a fixed geographic line but as a dynamic diagnostic frontier that moves with the climate state. Monitoring η^2 at threshold-proximal sites — Makassar, Port Moresby, and Darwin itself — on decadal intervals is a more defensible approach to maintaining the validity of operational MJO diagnostic products than assuming stationarity. The threshold identified here empirically provides the numerical target for that monitoring.

6.4 Generalisation to Other Large-Scale Forcing Modes

The active-versus-passive distinction is not MJO-specific. It constrains any diagnostic framework that conditions on the phase of a large-scale oscillatory forcing mode. The argument is general and its implications are immediate.

ENSO phase-conditioned rainfall diagnostics rest on the same implicit premise that CPA_{dry} tests explicitly: that statistically significant phase-rainfall association implies mechanistically grounded, phase-trackable predictive skill. The ENSO literature provides ready precedent for the same bifurcation. Sites where ENSO drives rainfall through direct SST modulation of local convection — equatorial Pacific islands, the Peru coast, the northern Australian monsoon region — satisfy the active-mechanism condition. Sites where apparent ENSO-rainfall association reflects Walker circulation adjustments, atmospheric bridge teleconnections, or moisture flux re-routing — East Africa, southern Africa, the Indian subcontinent — may exhibit strong phase-rainfall η^2 analogs while yielding no skill beyond persistence baselines. Ropelewski and Halpert (1987) and Trenberth et al. (1998) documented the geographic dependence of ENSO-rainfall associations, more importantly, Dai and Wigley (2000) and Grimm and Tedeschi (2009). The diagnostic implication — that mechanism type rather than association strength governs phase-conditional skill — has not been operationally formalised for ENSO any more than it had been for the MJO before this study.

The Quasi-Biennial Oscillation, the Indian Ocean Dipole (Saji et al.,1999), and low-frequency midlatitude teleconnections each involve both active local influence sites (Hoskins and Karoly., 1981,

The steady linear response of a spherical atmosphere to thermal and orographic forcing. J Atmos Sci 38:1179-1196) (Wallace and Gutzler., 1981, *Teleconnections in the geopotential height field during the Northern Hemisphere winter. Mon Wea Rev 109:784-812*) (Baldwin et al., 2001, *The quasi-biennial oscillation. Rev Geophus 39:179-229*) and passive remote influence sites within their statistical footprint. Testing whether phase-response diagnostics built on these modes yield skill at active versus passive sites — using the AUC lead-time framework applied here — would transform the coupling-contingency principle from an MJO-specific finding into a general constraint on phase-conditioned diagnostic methodology. CPA_{dry}'s architecture transfers directly: the only site-specific inputs are the phase index, the rainfall record, and the physically motivated suppressive phase classification. The test is therefore replicable at low cost. Whether the $\eta^2 \approx 5$–6% boundary applies at identical or shifted values to ENSO, QBO, or IOD phase diagnostics is an open quantitative question — and answering it would establish whether this threshold reflects a universal property of tropical convective organisation or a value specific to MJO dynamics.

---

7. Conclusions

Statistical coupling between MJO phase and local rainfall is necessary for diagnostic skill. It is not sufficient. The nature of the coupling — whether direct convective envelope modulation or remote teleconnection — is the additional governing condition. This paper establishes that condition formally, tests it across seven tropical sites, and quantifies where the boundary lies.

Five conclusions follow from the evidence.

CPA_{dry} provides genuine DPS precursor skill — AUC 0.69–0.76, rising with lead time to t+10–15 days — at Darwin ($\eta^2 = 7.5\%$) and Dili ($\eta^2 = 6.7\%$), where the MJO convective envelope passes directly overhead and active inhibitory dynamics operate locally. Skill exceeds rolling-rainfall baselines by +0.06 to +0.17 at the primary evaluation leads and survives independence tests ($\rho(CPA_{dry}, R\_60) < 0.05$). The rising-with-lead-time profile is the diagnostic signature of regime-scale forcing, not weather-scale noise.

Skill is absent at all remote-teleconnection sites, regardless of coupling magnitude. Colombo, at $\eta^2 = 11.2\%$ — the strongest-coupled site in the study — returns AUC = 0.50 across every lead time evaluated. The Colombo result is not an anomaly. It is the active-versus-passive principle's sharpest quantitative demonstration: coupling strength measures the statistical footprint of MJO influence, not the mechanism, and it is the mechanism that determines whether CPA_{dry} has anything to detect.

The suppression-enhancement asymmetry within active-modulation sites reflects the same principle operating within a single location. Suppression failure (AUC 0.69–0.76) is detectable because active dry-phase inhibition, when overridden, leaves a coherent dynamical signature that accumulates in a rolling window. Enhancement failure (AUC 0.52–0.55) is not detectable because wet-phase non-delivery is the stochastic absence of a permissive condition, not a coherent event with a prior state. Regime conditioning does not recover wet-phase skill, confirming the asymmetry is structural.

A coupling-contingency threshold near $\eta^2 \approx 5$–6% demarcates the transition from direct-envelope-passage to remote-teleconnection regimes. Below it, CPA_{dry} advantage over rolling-rainfall baselines is zero or negative at every site, regardless of coupling significance. Makassar ($\eta^2 = 4.0\%$) sits at the marginal boundary; the six-site linear fit excluding Colombo yields $R^2 = 0.87$. The threshold is not a statistical artefact. It marks the physical boundary below which MJO influence is too attenuated by

distance, barrier effects, or teleconnection diffusion to impose the locally acting inhibitory dynamics CPA_{dry} requires.

Both the threshold and the mechanism classification are climate-sensitive. Projected MJO amplitude intensification will push threshold-proximal sites — particularly Makassar — upward across the diagnostic boundary. Maritime Continent barrier weakening will shift eastern PNG sites toward diagnostic eligibility. Increasing positive IOD frequency will episodically suppress MJO convective organisation over northern Australia, pulling Darwin and Dili toward the threshold from above. The coupling-contingency principle, therefore, provides not only a current geographic criterion for diagnostic deployment but a framework for anticipating where that criterion will be gained or lost under future climate trajectories.

The field-level implication is direct. Phase-response diagnostic frameworks should not be deployed on the basis of η^2 alone. Mechanism classification — whether by the literature-supported physical pathway used here or by future observational or model-based approaches — must precede deployment. Sites with strong coupling but passive mechanisms are not candidates for CPA-type diagnostics. Applying such diagnostics to them does not merely underperform. It misleads.

Authors Declarations:

Conflict of interest/Competing interest:

The authors declare no known competing financial interests or personal relationships that could have appeared to influence the work reported in this paper.

Technical Compendium and Code availability:

The entire relevant Code has been uploaded as a separate document for transparency and clarity.
The authors have also submitted a detailed Technical Compendium that contains the entire paper's technical arguments and addresses the expected reviewers' concerns.
Any further code required shall be submitted as and when asked for.

References

Adames ÁF, Kim D, Clark SK, Ming Y, Inoue K (2017). Changes in the structure and propagation of the MJO with increasing CO_2. J Adv Model Earth Syst 9:1251–1268. https://doi.org/10.1002/2017MS000913

Annamalai H, and Slingo JM (2001). Active/break cycles: diagnosis of the intraseasonal variability of the Asian summer monsoon. Clim Dyn 18:85–102. https://doi.org/10.1007/s003820100161

Annamalai H, Slingo JM, Sperber KR, Hodges K (2003). The mean evolution and variability of the Asian summer monsoon: comparison of ECMWF and NCEP–NCAR reanalyses. Mon Wea Rev 131:1023–1039

Baldwin MP, Gray LJ, Dunkerton TJ, et al (2001). The quasi-biennial oscillation. Rev Geophys 39:179–229

Bergemann M, Jakob C, (2016). How important is tropospheric humidity for coastal rainfall in the tropics? Geophys Res Lett 43:5860-5868. https://doi/org/10.1002/2015GL067024.

Berhane F, Zaitchik B (2014) Modulation of daily precipitation over East Africa by the Madden–Julian Oscillation. J Clim 27:6016–6034. https://doi.org/10.1175/JCLI-D-13-00693.1

Berhane F, Zaitchik B, Dezfuli A (2015). Subseasonal-scale influence of the Madden–Julian Oscillation on daily precipitation and surface winds over West Africa and the eastern tropical Atlantic. J Clim 28:8540–8561. https://doi.org/10.1175/JCLI-D-14-00793.1

Birch CE, Webster S, Peatman SC, et al (2016). Scale interactions between the MJO and the western Maritime Continent. J Clim 29:2145–2163. https://doi.org/10.1175/JCLI-D-15-0557.1

Bosilovich MG, Akella S, Coy L, Cullather R, Draper C, Gelaro R, Kovach R, Liu Q, Molod A, Norris P, Wargan K, Chao W, Reichle R, Takacs L, Vikhliaev Y, Bloom S, Collow A, Firth S, Labow G, Partyka G, Pawson S, Reale O, Schubert SD, Suarez M (2015). MERRA-2: Initial evaluation of the climate. Technical Report Series on Global Modeling and Data Assimilation, Vol. 43. NASA/TM–2015–104606. NASA Goddard Space Flight Centre, Greenbelt.

Bui HX, Maloney ED (2018). Changes in Madden-Julian Oscillation precipitation and wind variance under global warming: Results from the CMIP5 intercomparison experiment. *Geophys Res Lett* 45:7148–7155. https://doi.org/10.1029/2018GL078504.

Cai W, Zheng X-T, Weller E, et al (2013). Projected response of the Indian Ocean Dipole to greenhouse warming. Nat Geosci 6:999–1007. https://doi.org/10.1038/ngeo2009

Chadwick R, Boutle I, Martin G (2013). Spatial patterns of precipitation change in CMIP5: why the rich do not get richer in the tropics. J Clim 26:3803–3822

Cohen J (1988). Statistical power analysis for the behavioural sciences, 2nd edn. Lawrence Erlbaum Associates, Hillsdale

Cowan T, Wheeler MC, de Burgh-Day C, Griffiths M (2023). Using the Madden–Julian Oscillation to forecast Australian and global precipitation. Bull Am Meteorol Soc 104:E1051–E1072. https://doi.org/10.1175/BAMS-D-21-0220.1

Dai A, Wigley TML (2000). Global patterns of ENSO-induced precipitation. Geophys Res Lett 27:1283–1286

DelSole T, Tippett MK (2022). Statistical methods for climate scientists. Cambridge University Press, Cambridge

DeMott CA, Klingaman NK, Woolnough SJ (2015). Atmosphere–ocean coupled processes in the Madden–Julian oscillation. Rev Geophys 53:1099–1154. https://doi.org/10.1002/2014RG000478

Domeisen DIV, White CJ, Afargan-Gerstman H, et al (2020). The role of the stratosphere in subseasonal to seasonal prediction: 1. Predictability of the stratosphere. J Geophys Res Atmos 125:e2019JD030920. https://doi.org/10.1029/2019JD030920

971 Feng J, Li J, Jin F-F, et al. (2020). Contrasting responses of the Hadley circulation to equatorially
972 asymmetric and symmetric sea surface temperature. J Clim 33:4443–4463.
973 https://doi.org/10.1175/JCLI-D-19-0695.1

974 Gelaro R, McCarty W, Suárez MJ, et al (2017). The Modern-Era Retrospective Analysis for Research
975 and Applications, Version 2 (MERRA-2). J Clim 30:5419–5454. https://doi.org/10.1175/JCLI-D-16-
976 0758.1

977 Gottschalck J, et al. (2010). A framework for assessing operational Madden-Julian Oscillation
978 forecasts: a CLIVAR MJO Working Group project. Bull Am Meteorol Soc 91:1247–1258

979 Grimm AM, Tedeschi RG (2009). ENSO and extreme rainfall events in South America. J Clim 22:1589–
980 1609

981 Hamada J-I, Yamanaka MD, Matsumoto J, et al (2002). Spatial and temporal variations of the rainy
982 season over Indonesia and their link to ENSO. J Meteorol Soc Jpn 80:285–310

983 Hanley JA, McNeil BJ (1982). The meaning and use of the area under a receiver operating
984 characteristic (ROC) curve. Radiology 143:29–36. https://doi.org/10.1148/radiology.143.1.7063747

985 Hendon HH, Liebmann B (1990). A composite study of onset of the Australian summer monsoon. J
986 Atmos Sci 47:2227–2240. https://doi.org/10.1175/1520-0469(1990)047<2227:ACSOO>2.0.CO;2

987 Hendon HH, Salby ML (1994). The life cycle of the Madden-Julian Oscillation. J Atmos Sci 51:2225–
988 2237

989 Hohenegger C, Stevens B (2013). Preconditioning deep convection with cumulus congestus. J Atmos
990 Sci 70:448–464. https://doi.org/10.1175/JAS-D-12-0079.1

991 Holland GJ (1986). Interannual variability of the Australian summer monsoon at Darwin: 1952–82.
992 Mon Wea Rev 114:594–604

993 Hoskins BJ, Karoly DJ (1981). The steady linear response of a spherical atmosphere to thermal and
994 orographic forcing. J Atmos Sci 38:1179–1196

995 Inness PM, Slingo JM (2006) The interaction of the Madden-Julian Oscillation with the Maritime
996 Continent in a GCM study. Q J R Meteorol Soc 132:1645–1667

997 Jayawardena IMSP, Samarasinghe SM, Perera AAS (2021). Influence of the Madden–Julian Oscillation
998 on rainfall over Sri Lanka. Int J Climatol 41:E2656–E2668. https://doi.org/10.1002/joc.6870

999 Jolliffe IT, Stephenson DB (eds) (2003). Forecast verification: A Practitioner's Guide in Atmospheric
1000 Science. Wiley, Chichester.

1001 Jones C, Waliser DE, Lau KM, Stern W (2004). The Madden–Julian Oscillation and its impact on
1002 Northern Hemisphere weather predictability. Mon Wea Rev 132:1462–1471.
1003 https://doi.org/10.1175/1520-0493(2004)132<1462:TMOAII>2.0.CO;2

1004 Katz RW, Parlange MB, Naveau P (2002). Statistics of extremes in Hydrology. Adv Water Resour
1005 25:1287–1304

Kemball-Cook S, Weare BC (2001). The onset of convection in the Madden-Julian oscillation. J Clim 14:780–793

Kiladis GN, Dias J, Straub KH, et al (2014). A comparison of OLR and circulation-based indices for tracking the MJO. Mon Wea Rev 142:1697–1715. https://doi.org/10.1175/MWR-D-13-00301.1

Kim HM, Kim D, Vitart F, et al (2017). MJO propagation across the Maritime Continent in the ECMWF ensemble prediction system. J Clim 29:3973–3990. https://doi.org/10.1175/JCLI-D-15-0862.1

Krishnamurthy V, Shukla J (2007). Intraseasonal and seasonally persisting patterns of Indian monsoon rainfall. J Clim 20:3–20. https://doi.org/10.1175/JCLI3981.1

Lau KM, Chan PH (1986). MJO convective envelope structure. Mon Wea Rev 114:1354–1367

Lavender SL, Matthews AJ (2009). Response of the West African monsoon to the Madden–Julian Oscillation. J Clim 22:4097–4116. https://doi.org/10.1175/2009JCLI2773.1

Lawrence DM, Webster PJ (2002). The boreal summer intraseasonal oscillation: relationship between northward and eastward movement of convection. J Atmos Sci 59:1593–1606

Lim Y, Son S-W, Kim D (2018). MJO prediction skill of the subseasonal-to-seasonal prediction models. J Clim 31:4075–4094. https://doi.org/10.1175/JCLI-D-17-0545.1

MacLeod DA, Bett PE, Scaife AA, et al. (2021) paper on East African short rains predictability or MJO influence on East African rainfall — possibly MacLeod D, et al. (2021) in *Geophys Res Lett* or *J Clim*.

Madden RA, Julian PR (1971). Detection of a 40–50 day oscillation in the zonal wind in the tropical Pacific. J Atmos Sci 28:702–708. https://doi.org/10.1175/1520-0469(1971)028<0702:DOADOI>2.0.CO;2

Madden RA, Julian PR (1972). Description of global-scale circulation cells in the tropics with a 40–50 day period. J Atmos Sci 29:1109–1123. https://doi.org/10.1175/1520-0469(1972)029<1109:DOGSCC>2.0.CO;2

Madden RA, Julian PR (1994). Observations of the 40–50-day tropical oscillation — a review. Mon Wea Rev 122:814–837. https://doi.org/10.1175/1520-0493(1994)122<0814:OOTDTO>2.0.CO;2

Mapes BE (2000). Convective inhibition, subgrid-scale triggering energy, and stratiform instability in a toy tropical wave model. J Atmos Sci 57:1515–1535. https://doi.org/10.1175/1520-0469(2000)057<1515:CISSTE>2.0.CO;2

Mason SJ, Graham NE (2002). Areas beneath the relative operating characteristics (ROC) and relative operating levels (ROL) curves: statistical significance and interpretation. Q J R Meteorol Soc 128:2145–2166. https://doi.org/10.1256/003590002320603584

Matthews AJ (2000). Propagation mechanisms for the Madden-Julian Oscillation. Q J R Meteorol Soc 126:2637–2651

Murphy AH (1988). Skill scores based on the mean square error and their relationships to the correlation coefficient. Mon Weather Rev 116:2417–2424.

May PT, Mather JH, Vaughan G, et al (2008). The Tropical Warm Pool International Cloud Experiment. Bull Am Meteorol Soc 89:629–645. https://doi.org/10.1175/BAMS-89-5-629

McBride JL, Nicholls N (1983). Seasonal relationships between Australian rainfall and the Southern Oscillation. Mon Wea Rev 111:1998–2004

Neelin JD, Peters O, Hales K (2009). The transition to strong convection. J Atmos Sci 66:2367–2384

Peatman SC, Matthews AJ, Stevens DP (2014). Propagation of the Madden–Julian Oscillation through the Maritime Continent and scale interaction with the diurnal cycle of precipitation. Q J R Meteorol Soc 140:814–825. https://doi.org/10.1002/qj.2161

Pepe MS (2003). *The Statistical Evaluation of Medical Tests for Classification and Prediction*. Oxford University Press, Oxford.

Pohl B, Camberlin P (2006). Influence of the Madden–Julian Oscillation on East African rainfall. I: Intraseasonal variability and regional dependency. Q J R Meteorol Soc 132:2521–2539. https://doi.org/10.1256/qj.05.104

Pohl B, Matthews AJP (2007). Observed changes in the lifetime and amplitude of the Madden–Julian Oscillation associated with interannual ENSO sea surface temperature anomalies. J Clim 20:2659–2674. https://doi.org/10.1175/JCLI4230.1

Qian JH (2008). Why precipitation is mostly concentrated over islands in the Maritime Continent. J Atmos Sci 65:1428–1441

Qian JH, Robertson AW, Moron V (2010). Interactions among ENSO, the monsoon, and diurnal cycle in rainfall variability over Java, Indonesia. J Atmos Sci 67:3509–3524. https://doi.org/10.1175/2010JAS3348.1

Ramage CS (1968). Role of a tropical “Maritime Continent” in the atmospheric circulation. Mon Wea Rev 96:365–370

Raymond DJ (1995). Regulation of moist convection over the west Pacific warm pool. J Atmos Sci 52:3945–3959. https://doi.org/10.1175/1520-0469(1995)052<3945:ROMCOT>2.0.CO;2

Raymond DJ, Herman MJ (2011). Convective quasi-equilibrium reconsidered. J Adv Model Earth Syst 3:M08003. https://doi.org/10.1029/2011MS000079

Reichle RH, Liu Q, Koster RD, et al (2017). Land surface precipitation in MERRA-2. J Clim 30:1643–1664. https://doi.org/10.1175/JCLI-D-16-0570.1

Romps DM, Kuang Z (2010). Nature versus nurture in shallow convection. J Atmos Sci 67:1655–1666. https://doi.org/10.1175/2009JAS3307.1

Ropelewski CF, Halpert MS (1987). Global and regional scale precipitation patterns associated with the El Niño/Southern Oscillation. Mon Wea Rev 115:1606–1626. https://doi.org/10.1175/1520-0493(1987)115<1606:GARSPP>2.0.CO;2

Roundy PE (2012). The spectrum of convectively coupled Kelvin waves and the Madden–Julian Oscillation in regions of low-level easterly and westerly background flow. J Atmos Sci 69:2107–2111. https://doi.org/10.1175/JAS-D-12-060.1

Roxy MK, Ritika K, Terray P, Masson S (2014). The curious case of Indian Ocean warming. J Clim 27:8501–8509

Rui H, Wang B (1990). Development characteristics and dynamic structure of tropical intraseasonal convection anomalies. J Atmos Sci 47:357–379. https://doi.org/10.1175/1520-0469(1990)047<0357:DCADSO>2.0.CO;2

Saji NH, Goswami BN, Vinayachandran PN, Yamagata T (1999). A dipole mode in the tropical Indian Ocean. Nature 401:360–363

Schlemmer L, Hohenegger C (2014). The formation of wider and deeper clouds as a result of cold-pool dynamics. J Atmos Sci 71:2842–2858. https://doi.org/10.1175/JAS-D-13-0170.1

Stackhouse PW Jr, Zhang T, Westberg D, et al (2018). POWER release 8 (with GIS applications) methodology (data parameters, sources, and validation). NASA Technical Report, Version 8.0.1. NASA Langley Research Centre, Hampton

Straub KH (2013). MJO initiation in the real-time multivariate MJO index. J Clim 26:1130–1151. https://doi.org/10.1175/JCLI-D-12-00074.1

Sultan B, Janicot S (2003). The West African monsoon dynamics. Part II: The “preonset” and “onset” of the summer monsoon. J Clim 16:3407–3427

Suematsu T, Martin ZK, Barnes EA, DeMott CA, Hagos S, Ham YG, Kim D, Kim H, Koh T-Y & Maloney ED, (2024). Incorrect computation of Madden-Julian oscillation prediction skill. (npj Climate and atmospheric science.)https://doi.org/10.1038/s41612-024-00687-1

Sun Q, Miao C, Duan Q, et al (2018). A review of global precipitation data sets: data sources, estimation, and intercomparisons. Rev Geophys 56:79–107. https://doi.org/10.1002/2017RG000574

Suppiah R (1997). Extremes of the Southern Oscillation phenomenon and rainfall of Sri Lanka. Int J Climatol 17:87–101

Thorncroft CD, Hoskins BJ (1994). An idealised study of African easterly waves. I: A linear view. Q J R Meteorol Soc 120:953–982

Tompkins AM (2001). Organisation of tropical convection in low vertical wind shears: the role of cold pools. J Atmos Sci 58:1650–1672

Trenberth KE, Branstator GW, Karoly D, Kumar A, Lau N-C, Ropelewski C (1998). Progress during TOGA in understanding and modelling global teleconnections associated with tropical sea surface temperature. J Geophys Res 103: 14291-14324.

Tsai Y-C, Maloney ED, Kim D and Camargo SJ, (2025). Unified Forecast System Prediction of the Madden-Julian Oscillation and Its Influence on East Pacific During Boreal Summer. (JGR Atmospheres)https://doi.org/10.1029/2024JD042904

Ventrice MJ, Wheeler MC, Hendon HH, et al (2013). A modified multivariate Madden–Julian Oscillation index using velocity potential. Mon Wea Rev 141:4197–4210. https://doi.org/10.1175/MWR-D-12-00327.1

Vitart F (2017). Madden–Julian Oscillation prediction and teleconnections in the S2S database. Q J R Meteorol Soc 143:2210–2220. https://doi.org/10.1002/qj.3079

Vitart F, Robertson AW (2018). The sub-seasonal to seasonal prediction project (S2S) and the prediction of extreme events. npj Clim Atmos Sci 1:3. https://doi.org/10.1038/s41612-018-0018-0

Wallace JM, Gutzler DS (1981). Teleconnections in the geopotential height field during the Northern Hemisphere winter. Mon Wea Rev 109:784–812

Webster PJ, Moore AM, Loschnigg JP, Leben RR (1999). Coupled ocean–atmosphere dynamics in the Indian Ocean during 1997–98. Nature 401:356–360. https://doi.org/10.1038/43848

Wheeler MC, Hendon HH (2004). An all-season real-time multivariate MJO index: development of an index for monitoring and prediction. Mon Wea Rev 132:1917–1932. https://doi.org/10.1175/1520-0493(2004)132<1917:AARMMI>2.0.CO;2

Wheeler MC, McBride JL (2005). Australian–Maritime Continent rainfall variability. In: Lau W, Waliser D (eds) Intraseasonal variability in the atmosphere–ocean climate system. Praxis, Chichester, pp 125–173

Wheeler MC, Zhu H, Sobel AH, et al (2009). Seamless precipitation prediction skill in the tropics and extra-tropics from a global model. Mon Wea Rev 137:3727–3742. https://doi.org/10.1175/2009MWR2814.1

Wilks DS (2019). Statistical methods in the atmospheric sciences, 4th edn. Elsevier Academic Press, Amsterdam

Wilson EA, Gordon AL, Kim D (2013). Indian Ocean interannual variability and its effect on MJO propagation in the Austral summer. J Clim 26:8578–8596. https://doi.org/10.1175/JCLI-D-12-00117.1

Woolnough SJ, et al (2000). The relationship between convection and sea surface temperature on intraseasonal timescales. J Atmos Sci 57:945–968

Yoneyama K, Zhang C, Long CN (2013). Tracking pulses of the Madden–Julian Oscillation. Bull Am Meteorol Soc 94:1871–1891. https://doi.org/10.1175/BAMS-D-12-00157.1

Zhang C (2005). Madden–Julian Oscillation. Rev Geophys 43:RG2003. https://doi.org/10.1029/2004RG000158